

High-Resolution Simulations of Decadal Climate Variability Impacts on Water Yield in the Missouri River Basin with the Soil and Water Assessment Tool (SWAT)

VIKRAM M. MEHTA AND KATHERIN MENDOZA

Center for Research on the Changing Earth System, Catonsville, Maryland

PRASAD DAGGUPATI AND RAGHAVAN SRINIVASAN

Texas A&M University, College Station, Texas

NORMAN J. ROSENBERG

Center for Research on the Changing Earth System, Catonsville, Maryland

DEBJANI DEB

Texas A&M University, College Station, Texas

(Manuscript received 20 March 2015, in final form 14 October 2015)

ABSTRACT

The Missouri River basin (MRB) is the largest river basin in the United States and is one of the most important agricultural regions in the world. Three decadal climate variability (DCV) phenomena—the Pacific decadal oscillation (PDO), the tropical Atlantic sea surface temperature (SST) gradient variability (TAG), and the west Pacific warm pool SST variability (WPWP)—substantially influence hydrometeorology in the MRB. The authors report on a simulation study with the Soil and Water Assessment Tool (SWAT) to estimate impacts on water availability in response to realistic values of PDO, TAG, and WPWP indices in approximately 13 500 hydrologic unit areas covering the MRB. SWAT, driven by hydrometeorological anomalies associated with positive and negative phases of PDO and TAG, indicated major impacts on water yields and streamflows, as much as $\pm 40\%$ of the average in many locations. Impacts of the WPWP index were smaller. Consistent with observations during 1949–2010, SWAT showed water flow increases of as much as 80% of the average, causing very wet periods when the positive phase of the PDO and the negative phase of the TAG at extreme amplitudes were superposed. Water flows decreased by a similar amount, resulting in severe to extreme droughts when the negative phase of the PDO and the positive phase of the TAG at extreme amplitudes were superposed. Thus, the combined and cumulative effects of these DCV phenomena on water flows, droughts, and wet periods in the MRB can be dramatic, with important consequences for all water-consuming sectors as well as for feedbacks to the climate system.

1. Introduction

Multiyear to decadal hydrologic cycles (DHCs), including extremely dry and wet spells, affect crop production; pasture and range conditions; urban and rural water systems; infrastructure; electricity generation; river navigation; recreation; livestock production and

health; ecological integrity; and, ultimately, regional and national economies (see, e.g., [Mehta et al. 2013a](#)). The recognition by decision-makers of increasing societal consequences of floods and droughts, some clearly attributable to DHCs, has prompted legislation at local, state, and national levels, encouraging improvements in water management and water use efficiency.

Floods cause loss of life and property in coastal regions and low-lying lands and often lead to public health hazards that threaten the lives of survivors. The effects of multiyear to decadal floods and droughts, however, are particularly dramatic in the agriculture sector, resulting in

Corresponding author address: Vikram M. Mehta, Center for Research on the Changing Earth System, 5523 Research Park Dr., Suite 315, Catonsville, MD 21228.
E-mail: vikram@crce.org

billions of dollars in crop losses around the world annually. Droughts affect more people worldwide than any other natural hazard (Wilhite 2000). Shortages of water for drinking and irrigation, consequent reductions in food production, and other stresses due to drought can contribute to social and political strife, civil wars, and international conflicts (Gleick 1993; Cooley et al. 2013). In addition to the need for information in times of immediate flood and drought emergency, planning for water, food, energy, and urban infrastructure development would benefit greatly, were it available, from reliable information on prospects for wet and dry periods extending one, two, or more decades into the future. But, skillful forecasts of this kind will require that the causes of DHCs and their impacts be better understood.

A substantial body of research has emerged in the last two decades focused on understanding causes and mechanisms of natural decadal climate variability (DCV; e.g., Meehl et al. 2009; Murphy et al. 2010) and its influences on terrestrial hydrology. Several DCV phenomena have been identified: these include the Pacific decadal oscillation (PDO; Mantua et al. 1997), the tropical Atlantic sea surface temperature (SST) gradient variability (TAG; Houghton and Tourre 1992; Mehta and Delworth 1995; Chang et al. 1997; Mehta 1998; Enfield et al. 1999), the west Pacific warm pool SST variability (WPWP; Wang and Mehta 2008), and decadal variability of interannual El Niño–La Niña events (Balmaseda et al. 1995; Kestin et al. 1998; Power et al. 1999; An and Wang 2000). These DCV phenomena have been identified in observational records and are associated with the occurrence of DHCs on land (Mehta 1998; Nigam et al. 1999; Hidalgo 2004; McCabe et al. 2004; Meehl and Hu 2006; Schubert et al. 2009; Mehta et al. 2011, 2014).

Simulation experiments with global earth system models (ESMs) have substantially clarified and reproduced the hypothesized impacts of DCV phenomena on precipitation and temperature in certain regions of the world (see, e.g., Schubert et al. 2009). While considerable progress has been made in understanding causes of DCV phenomena, understanding of DCV impacts on water availability and agriculture has not made a comparable progress even though numerous observational studies (see citations in the previous paragraph) have identified associations between them. Mehta et al. (2011, 2012) conducted two exploratory studies on a small number of watersheds in the Missouri River basin (MRB) that established the sensitivity of the basin's water and agriculture sectors to the impacts of DCV phenomena. Building on these previous studies, the present study is a part of a large program to develop a decadal climate and impacts simulation and prediction system for the MRB, to develop adaptation options for

water and agriculture sectors in the MRB using the decadal climate and impacts information, and to estimate the value of decadal climate and impacts information to the agriculture sector in the MRB. Global ESMs and a very high-resolution land-use–hydrology–crop model—the Soil and Water Assessment Tool (SWAT; Arnold and Allen 1993; Arnold et al. 1999)—are being used in this program. Preliminary results on decadal predictability of ocean-basin-averaged SSTs and decadal predictability of indices of the PDO, TAG, WPWP, and El Niño–La Niña phenomena are reported in Mehta et al. (2013b, 2015, manuscript submitted to *Climate Dyn.*) from this program. A dynamical–statistical technique for decadal hydrometeorological predictions being developed for the MRB—applied to southern Africa as a test case—is reported in Mehta et al. (2014). The research reported here was designed to simulate impacts of DCV phenomena on surface and groundwater in the MRB with SWAT. The responses of spring and winter wheat yields in the MRB to simulated DCV scenarios are not described here.

Importance of the MRB

1) LAND AND INDUSTRY

The importance of the MRB is described in detail in Mehta et al. (2011), so only a brief description is given here. The MRB covers approximately 1.3 million km², including a part or all of 10 U.S. states and two Canadian provinces; it is also home to 28 Native American tribes. Inhabitants of the basin depend on the Missouri River and its tributaries for irrigation, drinking water, industrial needs, hydroelectricity, navigation, recreation, and fish and wildlife habitat. The basin contains agrarian counties as well as more than 2000 urban communities, including large metropolitan areas such as Omaha, Nebraska; Kansas City, Missouri; and Denver, Colorado. The basin is a very important agricultural region, producing approximately 46% of U.S. wheat, 22% of its grain corn, and 34% of its cattle. Approximately 47.3 million ha are in cropland, 90% of them are entirely dependent on precipitation. Approximately 4.9 million ha are under irrigation, much of it dependent on water withdrawals from the Ogallala Aquifer, the most intensively used aquifer in the United States. In terms of economic importance, the approximate value of crops and livestock produced in the basin is over \$100 billion per year.

2) MANIFESTATIONS OF DECADAL CLIMATE VARIABILITY IN THE MRB

Much of the MRB—essentially all of it west of 100°W—lies within the Great Plains region of North

America and is semiarid in climate for the most part (Rosenberg 1987). East of 100°W, the land is included in what has been termed the “Prairie Provinces,” which is subhumid–humid in its climate. It is interesting to note that the early nineteenth-century explorers Zebulon Pike and Stephen Long passed through the Great Plains region in times of drought and referred to the region in their reports as a “desert” (Wishart 2004; Rosenberg 2007). Periodic droughts following European settlement of the Great Plains region led to repeated out-migrations from the region, the last major one in the 1930s. In the late nineteenth century, Powell (1879) recommended that irrigation be developed in this region to buffer the effects of recurrent droughts, and in the midst of the “Dirty Thirties,” a report to President Franklin D. Roosevelt (Cooke et al. 1936) proposed a wide variety of agronomic adaptations and policy adjustments to stabilize the region. All of these explorers and observers were certain that droughts (as well as wet spells) were a permanent feature of the region’s climate. None, of course, were aware that DCV forced by oceanic phenomena was a major cause.

In recent times, impacts of major global-scale DCV phenomena such as the PDO, TAG, and WPWP on U.S. climate are reasonably well documented and quantified by analyses of climate observations. There are indications that large-scale climate influences of the PDO (see, e.g., Ting and Wang 1997; McCabe et al. 2004; Mehta et al. 2011), TAG (Schubert et al. 2009; Mehta et al. 2011), and WPWP (Wang and Mehta 2008; Mehta et al. 2011) influence precipitation variability in the MRB at the decadal time scale. The Atlantic multidecadal oscillation is known to influence precipitation in the United States at multidecadal time scales (McCabe et al. 2004). Interannual ENSO variability explains less than 20% while decadal time scale variability explains approximately 40%–50% of the total precipitation, runoff, and streamflow variances within the basin (Guetter and Georgakakos 1993; Lins 1997; Cayan et al. 1998). The PDO and TAG acting individually explain approximately 20%–40% of precipitation variance in the basin, and 10%–20% is explained by the WPWP.

Gurdak et al. (2007) established a linkage between the PDO and groundwater recharge rates and mechanisms in the High Plains Aquifer that underlies much of the basin. These hydrologic variability estimates are also reflected in the percentage area of the basin under severe to extreme drought conditions. The fraction of the basin experiencing severe to extreme drought in the twentieth century has ranged from 20% to 60% or more at interannual to decadal time scales (Mehta et al. 2013a). Portions of the basin have also experienced a multiyear to near-decadal drought during the first

decade of the twenty-first century. The droughts have alternated with multiyear to decadal wet spells.

This paper is organized as follows. The introduction is followed in section 2 by a review of previous research and a statement of study objectives. The SWAT model, data used in this study, and experiment design are described in section 3; impacts of individual DCV scenarios on water yield and streamflow are described in section 4; impacts of multiple DCV scenarios on water yield are described in section 5; and impacts of extreme DCV scenarios are described in section 6. Discussion and conclusions are presented in section 7.

2. Background and objectives

The Hydrologic Unit Model of the United States (HUMUS; Srinivasan et al. 1993)–SWAT system has been used in studies relating agricultural and water resource management to climate change. Using this system, Thomson et al. (2003) simulated effects of various types of El Niño events on North American water resources. Rosenberg et al. (2003) simulated climate change scenarios and their impacts on irrigation water supply in North America. Jayakrishnan et al. (2005) simulated effects of management scenarios on water quantity and quality. Kannan et al. (2005, 2011) and Santhi et al. (2008) modified the HUMUS–SWAT system to use in the Conservation Effects Assessment Project to quantify environmental benefits of conservation practices used by private landowners participating in the U.S. Department of Agriculture (USDA) conservation programs.

In an exploratory study, Mehta et al. (2011) applied the HUMUS–SWAT system to 75 widely scattered locations in the MRB in order to explore how the PDO, TAG, and WPWP affect net water availability.¹ Hydrometeorological anomalies associated with positive and negative phases of the three DCV phenomena at their average amplitudes were used to drive HUMUS–SWAT. In the positive phase of the PDO, the tropical–subtropical Pacific SSTs are above average and the midlatitude Pacific SSTs are below average; in the negative phase of the PDO, the tropical–subtropical Pacific SSTs are below average and the midlatitude Pacific SSTs are above average (Mantua et al. 1997). In the positive phase of TAG, tropical North Atlantic SSTs are above average and the tropical South Atlantic SSTs are below

¹ Net water availability was defined as the amount of water available for runoff and groundwater percolation that was obtained as the arithmetic difference between precipitation and evapotranspiration.

average; in the negative phase of TAG, tropical North Atlantic SSTs are below average and the tropical South Atlantic SSTs are above average (Mehta 1998). The WPWP is above average in the positive phase and below average in the negative phase (Wang and Mehta 2008). The HUMUS–SWAT simulations revealed major impacts, with locally specific variations as large as $\pm 50\%$ of average net water availability. For typical values of the three DCV indices (Mehta et al. 2011), basin-aggregated net water availabilities differed substantially between positive and negative phases of the PDO, TAG, and WPWP.

The results of our exploratory studies of DCV impacts on net water availability (Mehta et al. 2011) and crop yields (Mehta et al. 2012) in the MRB were reported to over 125 farmers, water managers, policymakers, and other stakeholders in several organized workshops held in the MRB. While the results were very interesting to these stakeholders and policymakers, they indicated (Mehta et al. 2013a) that, to be useful for planning and other purposes, climate and impacts information must be provided at the spatial and temporal resolutions required by each societal sector. The surface area of each watershed in our exploratory study ranged from 800 to 13 000 km², with the average watershed area being 4500 km². Thus, our study included only 337 500 km² surface area out of the total of 1.322 million km² area of the MRB, and the exploratory study used only minimally calibrated and validated HUMUS–SWAT system. Therefore, in our current program on decadal climate and impacts simulation and prediction, mentioned in the introduction, we are using a very high-resolution version of SWAT that is also much improved in other ways, as described in section 3a. The spatial resolution of SWAT employed in these studies was determined by the spatial resolution of observed, gridded hydrometeorological data, available for a sufficiently long period of time, to drive SWAT; these data are described in section 3b. Employing the very high-resolution SWAT allows us to aggregate water and crop yields data at any coarser-resolution levels from local watersheds to the entire MRB as required by stakeholders and policymakers. Also, the PDO, TAG, and WPWP indices were at or above their absolute average values in 32, 27, and 27 years, respectively, during the 61-yr (1949–2010) study period. Therefore, simulating individual and simultaneous impacts of average amplitudes of these DCV phenomena would not only provide insights into how DCV phenomena impact water and crop yields, but also allow us to provide guidance to stakeholders and policymakers in the MRB on impacts of relatively frequently occurring DCV phenomena. Additionally, simulating impacts of extreme

amplitudes of these DCV phenomena would allow us to provide “best/worst case scenarios” to the stakeholders and policymakers.

Therefore, in the study reported here, the overarching objective is to simulate the influences of various states and combinations of the PDO, TAG, and WPWP on surface and groundwater contributions to water yields and stream/river flows in the MRB. Specifically, the following questions are addressed with the very high-resolution and advanced version of SWAT:

- 1) What are the impacts of hydrometeorological anomalies associated with positive and negative phases and average amplitudes of PDO, TAG, and WPWP individually on surface and groundwater contributions to water yields and stream/river flows in the MRB?
- 2) What are the impacts of hydrometeorological anomalies associated with various combinations of PDO, TAG, and WPWP at their average amplitudes in both positive and negative phases on surface and groundwater contributions to water yields and stream/river flows in the MRB?
- 3) What are the impacts on surface and groundwater contributions when the three DCV phenomena are at their extreme amplitudes in both their positive and negative phases?

3. SWAT, data, and experiment design

a. SWAT

SWAT, developed by the USDA’s Agricultural Research Service (ARS), is a physically based, spatially distributed watershed model used to evaluate long-term impacts of land management practices on water resources over a range of scales (Srinivasan and Arnold 1994; Rosenthal et al. 1995; Spruill et al. 2000; Weber et al. 2001; Santhi et al. 2001; Di Luzio et al. 2002; Jayakrishnan et al. 2005; Gassman et al. 2014). SWAT is efficient in terms of computational power and time and can simulate processes of interest in very large basins over long periods of time. Major components of SWAT include hydrology, weather, sedimentation, soil temperature, crop growth, nutrients status in soil and water, agricultural management, and pesticides, and each component is further divided into subcomponents. Moreover, a watershed is divided into multiple sub-watersheds, which are then further subdivided into hydrologic response units (HRUs) characterized by homogeneous land use, management, and soil characteristics. SWAT simulates the overall hydrologic balance for each HRU with a daily time step, and model output is available in daily, monthly, and annual time

steps. Detailed descriptions of the methods used in modeling these components and subcomponents can be found in [Arnold et al. \(1999\)](#) and [Neitsch et al. \(2005\)](#).

The HUMUS–SWAT system for the MRB was originally set up at a coarse resolution of eight-digit hydrologic unit codes (HUCs; 310 subwatersheds in the MRB with an average area of 3000 km² each) and was minimally calibrated and validated using average annual observed streamflow ([Arnold et al. 1999](#); [Rosenberg et al. 2003](#)). The geographic details applied in previous versions of the HUMUS–SWAT system do not adequately serve many water resource investigations and management needs. Moreover, investigations using higher-resolution subbasins (12-digit watersheds) would help local, state, and federal agencies within the United States to develop the framework needed for watershed management decisions, as also revealed by our interactions with stakeholders and policymakers in the MRB. Keeping this in mind, we use 12-digit watersheds (average area of 100 km² each) in the very high-resolution SWAT developed for the MRB. Details of the very high-resolution model development and its calibration and validation are described in [Daggupati et al. \(2016\)](#), so only a brief description is given here.

Developing a physically based, very high-resolution hydrologic model for vast basins like the MRB is a difficult task because of the large amounts of input information required and the complexity of their integration ([Santhi et al. 2008](#)). Therefore, the MRB was first divided into three parts (upper, middle, and lower MRB) to simplify the modeling effort and increase simulation speed. Upper MRB encompasses the drainage areas of the Yellowstone and upper Missouri Rivers. Middle MRB includes the drainage areas of the Platte, James, and middle Missouri Rivers. Lower MRB includes the drainage areas of the Kansas and lower Missouri Rivers. These three parts of the MRB were simulated individually. Because of their large areas (upper, 473 133 km²; middle, 554 770 km²; and lower, 294 243 km²), spatial variability within each part was considered in its calibration, including variability of land use, vegetation cover, elevation, and climate. These three parts of the MRB were hydrologically connected by inputting flow from the upper to the middle and from the middle to the lower parts. Then, the MRB was further divided into 11 regions, and a “headwater catchment” (consisting of multiple 12-digit watersheds with an observed streamflow gauge, no reservoirs, and no major manual water abstraction) was selected in each region and was calibrated for crop and water yields. The parameters from the calibrated headwater catchment

were extrapolated to other subwatersheds in the region to complete a comprehensive calibration.

ArcSWAT 2012 (revision 612) for ArcGIS (version 10) interface ([Winchell et al. 2007](#)) was used in this study. Several changes in interface and model routines were made to ArcSWAT 2012 to apply it for simulation of large basins such as the MRB.

The ArcSWAT interface user-defined watershed boundary and stream option was used to input processed 12-digit HUCs, the National Hydrography Dataset, and 30-m (3 arc s) digital elevation model data for each river basin to provide watershed and topographic parameter estimation.

Land-use data covering the basin were obtained from 2010 and 2011 Cropland Data Layers (CDLs). Several postprocessing techniques were developed to combine CDL and MODIS irrigated land layers to prepare a land-use/land-cover map at 30-m resolution that has crop rotations, and irrigated lands are considered in the delineation. The land-use data provide spatial information on where particular crops are grown. Data on associated management practices such as crop variety, crop rotation, planting and harvesting dates, and fertilizer and irrigation rates must be provided by the user. To obtain such spatial management data for the entire MRB would be an overwhelming task even if such data were readily accessible. Therefore, in this study, we made simplifying assumptions regarding management practices.

Growth of major dryland and irrigated crops grown in the basin (such as corn, soybean, and winter and spring wheat) are represented in SWAT using plant growth algorithms based on heat unit scheduling. SWAT simulates plant growth using a heat unit approach where plant heat units are defined as the difference between plant base temperature and daily temperature, summed for all days when temperature is above the base temperature. SWAT specifies a “planting” (growth start) operation and a “kill” (stop growth and convert to residue) operation for each selected plant species. The timing of management operations is expressed in fractions of total heat units required for crop maturity. For example, the fraction of total heat units for harvest operation is 1.16. The fraction is greater than 1.0 because corn is allowed to dry prior to harvesting. Fertilizer and irrigation applications are triggered when a specified “heat units to maturity” is reached. In this study, an automatic fertilizer routine was used to simulate fertilizer application, a function of user-specified nitrogen stress. For irrigated crops, an auto irrigation routine was used to supply water as a function of user-specified water stress threshold. Rangeland and forest occur across the basin. Care was taken such that the “real world” plant

species of rangeland and forest are represented spatially in SWAT. The State Soil Geographic (STATSGO; NRCS 1994) 1:250 000 scale map was used in this study. All soil properties needed for the very high-resolution SWAT were extracted from the STATSGO layer and distributed with the ArcSWAT software.

HRUs are the basic building blocks for SWAT that have homogeneous hydrologic characteristics. Through the ArcSWAT interface, land use, soil, and slope layers were overlaid to create unique combinations of HRUs within the upper, middle, and lower MRB. The slope classes used for this process were 0%–4%, 4%–8%, and greater than 8%. A total of 103 793, 160 267, and 105 569 HRUs were derived in the upper, middle, and lower MRB, respectively.

There are numerous small, medium, and large reservoirs within the MRB. Reservoir data—such as size, area, and volume impounded—were obtained from the National Inventory Dataset (from nid.usace.army.mil) and converted into SWAT-readable input format. There are 37, 38, and 32 reservoirs in the upper, middle, and lower MRB, respectively. Major reservoirs on the Missouri River (main stem) were simulated using the daily reservoir outflow approach where the observed daily streamflow data from a gauge downstream of the reservoir were input into SWAT. For all other reservoirs, the simulated control outflow approach was used because of a lack of adequate reservoir release data and the complexity involved in simulating each reservoir operation.

SWAT was first calibrated for crop yield and then for hydrology. Simulated yields of dryland corn, soybean, winter wheat, and spring wheat and of irrigated corn and soybean were calibrated against actual yields estimated by the USDA's National Agricultural Statistics Service. Simulated and observed crop yields were in close agreement in headwater catchments, with bias and normalized root-mean-square errors less than 20%. Then streamflows were calibrated over a 10-yr period using available, continuous U.S. Geological Survey (USGS) streamflow records at the gauge outlet of the headwater catchments. Average annual water balance was calibrated first, followed by monthly temporal calibration using the automated Sequential Uncertainty Fitting, version 2 (SUFI-2), routine in the SWAT Calibration and Uncertainty Programs (SWAT-CUP; [Abbaspour et al. 2007](#)) within SWAT. Quantitative criteria recommended by [Moriassi et al. \(2007\)](#) were used to evaluate performance of the monthly and annual simulations. Additionally, the strength of calibration and uncertainty analysis were evaluated using criteria recommended by [Abbaspour et al. \(2007\)](#). Simulated and observed water yields were in close agreement for 9 of the 11 selected headwater catchments. The coefficient

TABLE 1. NSE and r^2 in headwater catchments.

Basin	Headwater catchment	r^2	NSE
Upper MRB	Marias	0.79	0.77
	Little Muddy	0.71	0.60
	Big Dry	0.65	0.64
	Big Hole	0.74	0.70
Middle MRB	Cherry	0.73	0.70
	Up Northloop	0.09	-1.34
	James	0.76	0.65
Lower MRB	West Fork Big Blue	0.54	0.40
	West Nishaboshana	0.84	0.75
	Up Saline	0.89	0.87
	Big Penny	0.80	0.68

of determination r^2 and Nash–Sutcliffe efficiency (NSE) for each headwater catchment are given in [Table 1](#). Two headwater catchments—Up Northloop and West Fork Big Blue—where the r^2 and NSE values are not satisfactory are located on top of the Ogallala Aquifer recharge zone, where the streams are fed mainly by groundwater recharge. The current groundwater routines in SWAT do not simulate surface–ground–streamflow interactions, hence the unsatisfactory results in these two headwater catchments. Spatial validation of water yields showed that the model simulations were satisfactory in natural-flow streams, but less so in streams where surface–ground–streamflow interactions are large and/or reservoirs are found upstream of the streamflow gauges. Overall, in the context of large-scale modeling studies, the calibration results were satisfactory.

b. Data

Data on hydrometeorological forcings (forcings hereafter) for use in SWAT from 1950 to 1999 were from [Maurer et al. \(2002\)](#). The forcings included daily precipitation rate, maximum and minimum air temperature, wind speed, and relative humidity—all at 2-m height. This dataset is available for North America at a resolution of $0.125^\circ \times 0.125^\circ$ latitude–longitude (from www.jisao.washington.edu/data).

To derive the PDO index (PDOI), we used the Hadley Centre Sea Ice and Sea Surface Temperature dataset, version 1 (HadISST1), from 1900 to 1981 ([Rayner et al. 2003](#)) and Optimum Interpolation SST (versions 1 and 2; [Smith and Reynolds 2004](#)) from January 1982 to December 2010. We derived standardized values of the PDO index as the leading principal component of monthly SST anomalies in the North Pacific Ocean poleward of 20°N . Monthly and global-average SST anomalies were subtracted from the principal component time series to separate PDO variability from any global warming signal that may be present in the data. The TAG index was derived as the difference between

monthly average SST anomalies in the tropical North Atlantic (5.5°–23.5°N, 15°–57.5°W) and tropical South Atlantic (0°–20°S, 10°E–30°W). The WPWP index was derived by averaging SST anomalies in the box 20°S–20°N, 90°E–180°. A linear trend was removed from the entire time series.

c. Preparation of idealized, individual, and multiple DCV scenarios

Twenty-nine SWAT experiments were designed to address the questions posed in section 2. The first question was addressed with six experiments in which statistically derived forcings for positive and negative phases of the PDO, TAG, and WPWP indices at their average values during the 1949–2010 period were used to drive SWAT. Then, these forcings for both positive and negative phases of the three DCV indices were superposed in eight combinations (two phases and three DCV phenomena; $2^3 = 8$ combinations). These eight experiments addressed the second question. To further test the sensitivity of water yields to extremes in the three DCV indices (the third question), forcings associated with extreme values of the PDO, TAG, and

TABLE 2. Monthly amplitudes of DCV phenomena in each scenario.

	PDO			TAG			WPWP		
	Avg	Max	Min	Avg	Max	Min	Avg	Max	Min
Jan	0.69	1.78	-1.26	0.25	0.59	-0.83	0.08	0.15	-0.27
Feb	0.74	1.68	-1.51	0.30	0.74	-0.92	0.08	0.17	-0.22
Mar	0.76	1.82	-1.26	0.31	0.89	-0.75	0.08	0.19	-0.22
Apr	0.70	1.41	-1.49	0.33	0.85	-0.90	0.07	0.19	-0.17
May	0.78	1.93	-1.50	0.32	0.88	-1.02	0.06	0.17	-0.14
Jun	0.61	1.76	-1.34	0.27	0.62	-0.83	0.06	0.12	-0.19
Jul	0.67	1.71	-1.18	0.20	0.36	-0.68	0.06	0.12	-0.15
Aug	0.56	1.14	-0.98	0.18	0.36	-0.56	0.06	0.14	-0.15
Sep	0.48	1.19	-1.01	0.18	0.32	-0.57	0.07	0.18	-0.17
Oct	0.53	1.12	-0.92	0.20	0.34	-0.62	0.07	0.19	-0.21
Nov	0.44	1.16	-0.86	0.19	0.35	-0.55	0.07	0.16	-0.21
Dec	0.46	1.64	-0.97	0.21	0.57	-0.61	0.07	0.16	-0.21

WPWP indices in the 1949–2010 period were used to drive SWAT in six experiments. Finally, these forcings associated with extreme values of the three indices were superposed into eight combinations of the three DCV indices. To compare with the DCV scenario experiments, one climatology experiment was run at each local watershed in which SWAT was forced by monthly

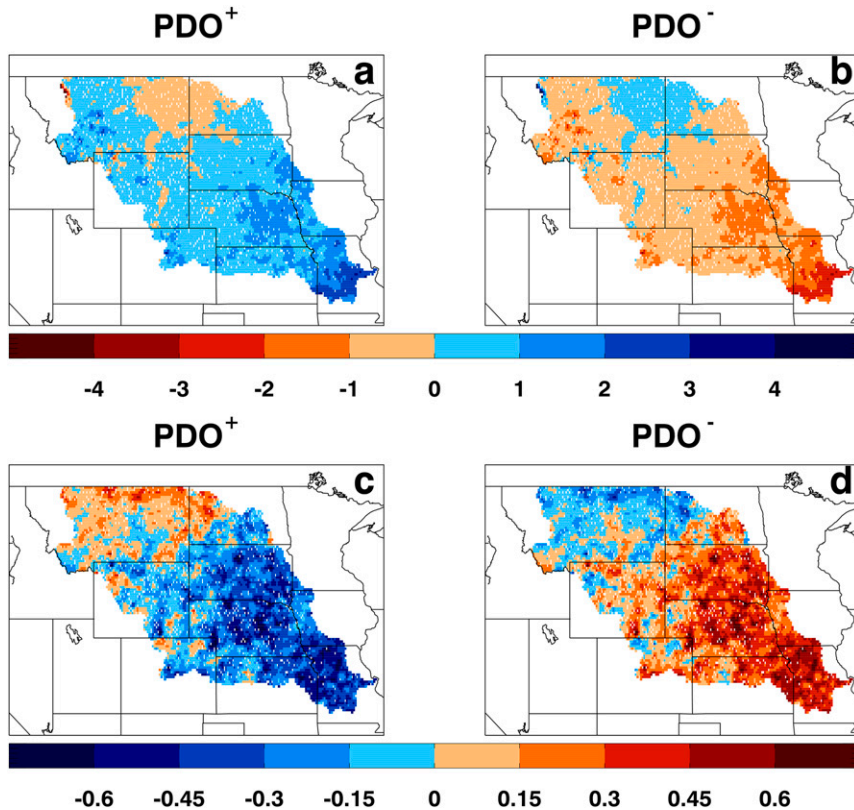


FIG. 1. Annual-average precipitation (mm day^{-1}) and daily max temperature ($^{\circ}\text{C}$) anomalies associated with (a) PDO^+ , precipitation; (b) PDO^- , precipitation; (c) PDO^+ , temperature; and (d) PDO^- , temperature.

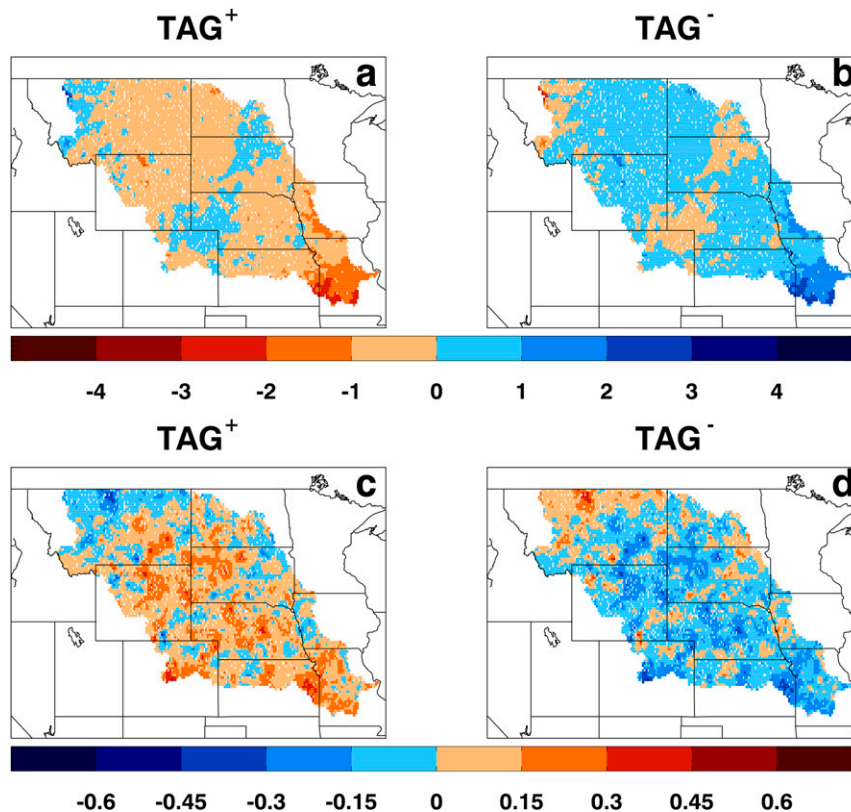


FIG. 2. Annual-average precipitation (mm day^{-1}) and daily max temperature ($^{\circ}\text{C}$) anomalies associated with (a) TAG^+ , precipitation; (b) TAG^- , precipitation; (c) TAG^+ , temperature; and (d) TAG^- , temperature.

values of hydrometeorological variables averaged over 1990–99 in the watershed.

As indicated in section 2, our earlier modeling study in the MRB with the HUMUS–SWAT system encompassed only 75 sites. Upon calibration and validation of the new high-resolution version of SWAT, the number of locations was increased to include approximately 13 500 representing the entire MRB, with each location corresponding to a local watershed.

There were two components of the DCV forcing scenarios at each location. One was an average annual cycle of monthly forcing and the other was a monthly forcing anomaly associated with an individual DCV phenomenon or with combined DCV phenomena. These two components were arithmetically added to produce the total forcing to drive SWAT. As mentioned in section 3b, the forcings included daily precipitation rate, maximum and minimum air temperature, wind speed, and relative humidity—all at 2-m height. The average annual cycle of monthly forcing was calculated for each location by averaging daily data at that location over the 10-yr period 1990–99 because that was the last decade for which data were available on all variables. For example, R_{Jan} was the

average value of precipitation rate R over 10 Januaries from 1990 to 1999 at each location.

To associate forcing anomalies with DCV phenomena, all monthly forcings and DCV indices for the 1950–99 period were low-pass filtered to allow periods equal to or longer than 8 years to pass through with no attenuation of amplitude; amplitudes of all periods shorter than 8 years were set to zero. Then a regression analysis was carried out between each of the five filtered monthly forcings and filtered monthly PDO, WPWP, and TAG indices. Linear regression equations were fitted for each calendar month between each forcing and each DCV index at each location. An example of the procedure, a regression equation for January, fitted between low-pass-filtered January precipitation anomaly R' and the PDOI for the 1950–99 period, is given here:

$$\begin{aligned} R'(\text{year, January}) &= [m_{\text{PDO}}(\text{January})][\text{PDOI}(\text{year, January})] \\ &\quad + C_{\text{PDO}}(\text{January}). \end{aligned}$$

Here, m_{PDO} is the slope and C_{PDO} is the intercept of the regression line. Two tests were used (Mehta et al. 2012)

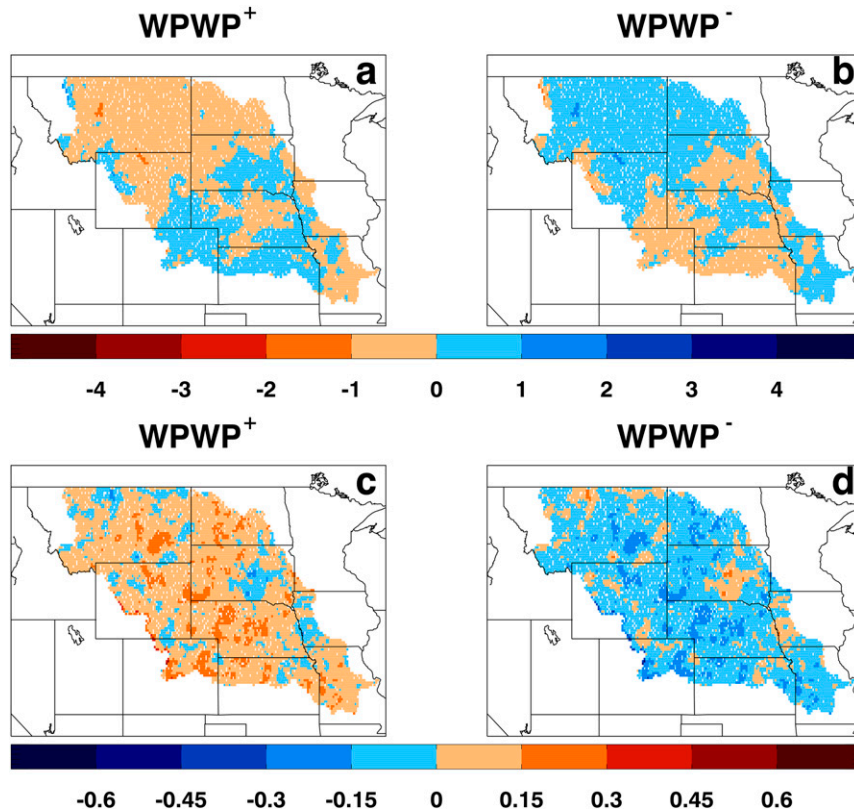


FIG. 3. Annual-average precipitation (mm day^{-1}) and daily max temperature ($^{\circ}\text{C}$) anomalies associated with (a) WPWP^+ , precipitation; (b) WPWP^- , precipitation; (c) WPWP^+ , temperature; and (d) WPWP^- , temperature.

to determine the significance of the slopes and intercepts—the r^2 test for the “goodness of fit” of the regression model and the Student’s t test for the statistical significance of the regression coefficients (Press et al. 2007). The r^2 value represents the variance of a forced variable explained by the regression. The t test determines if the resulting coefficients from the regression are distinguishable from zero. The monthly r^2 values for precipitation rate over 50 years at each location in the MRB vary from 0.1 to 0.6–0.7 individually for the PDO and the TAG. The values are somewhat smaller for the WPWP. The annual-average r^2 value for precipitation rate, averaged over the entire MRB, is approximately 0.25 for the PDO and the TAG and approximately 0.1 for the WPWP. The r^2 values for daily maximum and minimum temperature are larger for each of the three DCV indices. Based on the t test, it was found that patterns of 95% significance are similar to those of the r^2 values. At specific locations in the MRB, this is also evident with all significant t -test areas coinciding with r^2 areas, with the latter values approximately greater than or equal to 0.1. Thus, results of these two significance tests were generally found to be satisfactory.

In the next step, using these regression coefficients, forcing anomalies corresponding to the average positive or average negative value of the corresponding DCV index were generated. For example, m_{PDO} and C_{PDO} for January were used, along with an average positive value of PDOI (PDOI^+) over the 1950–99 period, to create the precipitation anomaly R_{PDOI^+} corresponding to PDOI^+ for January:

$$R_{\text{PDOI}^+}(\text{January}) = [m_{\text{PDO}}(\text{January})][\text{PDOI}^+(\text{January})] + C_{\text{PDO}}(\text{January}).$$

Finally, to complete each DCV-related climate scenario, the January precipitation rate anomaly $R_{\text{PDOI}^+}(\text{January})$ was added to the corresponding average monthly climatology R_{Jan} , producing the total precipitation rate $R_{\text{PDOI}^+}(\text{January})$ at a particular location associated with average positive PDO index:

$$R_{\text{PDOI}^+}(\text{January}) = R_{\text{Jan}} + R_{\text{PDOI}^+}(\text{January}).$$

This procedure was repeated at all locations, all calendar months from January to December, and all

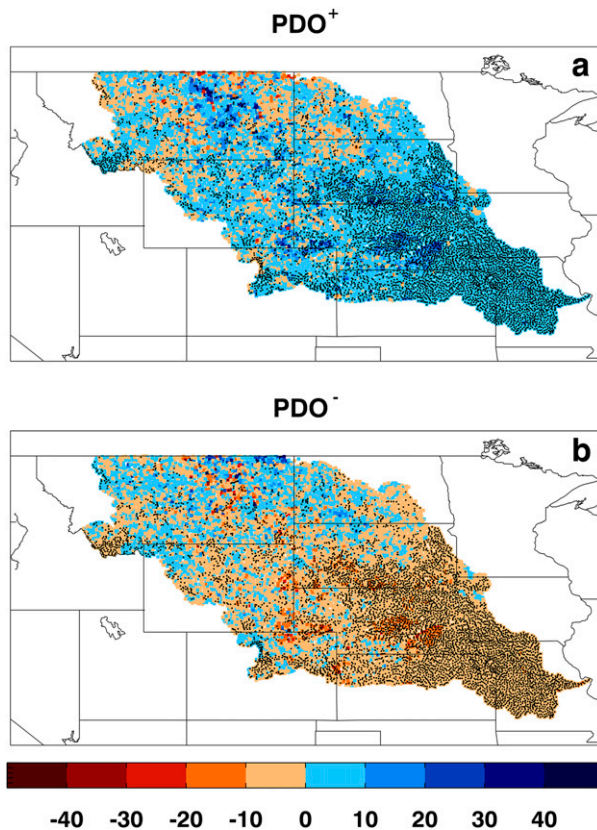


FIG. 4. SWAT-simulated annual-average water yield (% change from climatology) in the MRB in (a) PDO^+ and (b) PDO^- phases. Black dots show locations of 95% significance.

forcings to produce an annual cycle of forcing data for the PDO^+ scenario. This set of idealized DCV scenarios is titled individual DCV scenarios (IDSs). In the scenario set titled IDS-Avg and containing six members, PDOI^+ and other DCV indices were the average value of each index. In the scenario set titled IDS-Extremes, also containing six members, maximum positive and minimum negative values of each index in the 1949–2010 period were used.

In the second set of scenarios, named combined DCV scenarios (CDS), forcings corresponding to positive and negative phases of the three individual DCV phenomena, derived as explained for the IDSs, were arithmetically added. There are eight combinations of three DCV phenomena (PDO, TAG, and WPWP) and two phases (positive and negative). These eight combinations are (PDO^+ , TAG^+ , WPWP^+), (PDO^- , TAG^- , WPWP^-), (PDO^+ , TAG^- , WPWP^+), (PDO^+ , TAG^- , WPWP^-), (PDO^- , TAG^+ , WPWP^+), (PDO^- , TAG^+ , WPWP^-), (PDO^+ , TAG^+ , WPWP^-), and (PDO^- , TAG^- , WPWP^+). Forcing anomalies at the average amplitude associated with each of the eight scenarios were superimposed on their climatological values—as in the IDS-Avg

scenarios—and the total forcings were used as input to SWAT; this subset is referred to as CDS-Avg. The maximum and minimum values of the three DCV indices in the 1949–2010 period were used in the other subset titled CDS-Extremes, also containing eight scenarios. Thus, a total of 29 (28 DCV scenarios and 1 climatology scenario) scenarios were formed. The monthly amplitudes of each of the DCV scenarios are given in Table 2.

A simulation experiment for each scenario in each set was run with SWAT forced by 12 months of forcings for 10 years. The total monthly forcings were provided as an input to the weather generator in SWAT whose daily output was provided as an input to the SWAT simulations. Thus, we obtained 10 annual samples of output variables for each scenario. Results averaged over the 10 samples are described in this paper. Results were analyzed at all locations. A z-score test (Spiegel and Stephens 2007) was used to show locations where differences between positive and negative phases of each DCV phenomenon (e.g., between PDO^+ and PDO^-) were 95% significant. The z-score value represents how many standard deviations an element is from the average and is found by dividing the difference of the anomalous positive and negative scenario averages by the standard deviation of the difference of the anomalous scenario distributions.

In figures showing impacts of various scenarios in subsequent sections, each of the 12-digit locations in the MRB is represented by a symbol (square) placed at the center latitude–longitude of the location. Some symbols overlap because of the close proximity of the center points of neighboring locations, while others are spaced farther apart, resulting in blank (white) space between locations. Black dots mark locations where differences in water yield are significant.

4. Impacts of individual decadal climate variability scenarios

a. Hydrometeorological anomalies associated with each scenario

Regression analyses showed that substantial precipitation and temperature anomalies in the MRB are associated with both phases of the PDO. Figure 1a shows that precipitation anomalies associated with the positive phase of the PDO (PDO^+) are generally positive in the MRB, except in the north-central part of the basin, where they are negative. Figure 1b shows that precipitation anomalies associated with the negative phase of the PDO (PDO^-) are generally negative, except in the north-central part of the basin. The largest

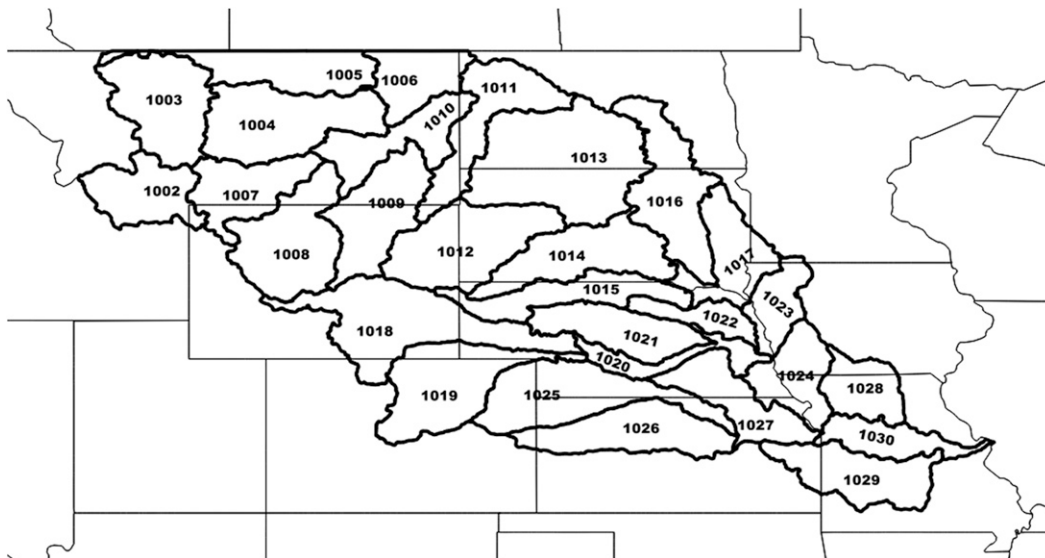


FIG. 5. Map of four-digit subbasins in the MRB.

precipitation anomalies associated with PDO^+ range from 3 to 5 mm day^{-1} and from -3 to -4 mm day^{-1} with PDO^- . Under PDO^+ , daily maximum temperature T_{max} (Fig. 1c) is below average by -0.3° to -0.6°C , except in small areas in Wyoming, Colorado, and western Nebraska, and in northern Kansas, most of Montana, and western North Dakota.

Under PDO^- conditions, T_{max} (Fig. 1d) is above average by 0.3° – 0.6°C almost everywhere in the basin except in Montana and western North Dakota. Under the positive phase of TAG (TAG^+), precipitation (Fig. 2a) is below average by 1–2 mm day^{-1} almost everywhere in the MRB. Almost everywhere in the basin, these precipitation changes are associated with T_{max} increases from near 0° to 0.3°C (Fig. 2c), except for a few locations in central South Dakota, northern Wyoming, Nebraska, Kansas, and northeastern Colorado, where T_{max} is lower by a few tenths of a degree Celsius. In the negative phase of TAG (TAG^-), precipitation (Fig. 2b) increases approximately 1–3 mm day^{-1} everywhere except for a few locations in South Dakota and Nebraska. The T_{max} is generally below average everywhere, ranging from near -0.1° to -0.3°C (Fig. 2d). Precipitation anomalies tend to be less dramatic under both phases of WPWP than they are under PDO or TAG, and generally differed in sign between its phases as for PDO and TAG. In southeastern MRB (Missouri and southwestern Iowa), precipitation anomalies are from -1 to 1 mm day^{-1} in the positive phase of WPWP ($WPWP^+$; Fig. 3a) and the negative phase of WPWP ($WPWP^-$; Fig. 3b), but with opposite signs in the two phases. In the central MRB (Nebraska and northern Kansas), precipitation

anomalies are from 0 to 1 mm day^{-1} in $WPWP^+$ and from 0 to -1 mm day^{-1} in $WPWP^-$. In the northwestern portions of the MRB (western South Dakota, North Dakota, Wyoming, and Montana), precipitation anomalies are largely negative, ranging from near 0 to 2 mm day^{-1} in $WPWP^+$ and from 0 to -1 mm day^{-1} in $WPWP^-$. The T_{max} anomalies range from 0° to 0.3°C in $WPWP^+$ (Fig. 3c) and from -0.1° to -0.3°C in $WPWP^-$ (Fig. 3d).

Thus, all six individual DCV scenarios display some influence on the hydrometeorology of the MRB, with PDO influences being the most substantial. The PDO^+ (PDO^-) phase is associated with wetter (drier) and cooler (warmer) temperatures over most of the southern half of the basin, with opposite sign anomalies elsewhere. Generally, the effects of positive and negative phases of TAG on the basin hydrometeorology are the opposite of those that occur under positive and negative phases of the PDO. The TAG^- (TAG^+) phase is associated with wetter (drier) and cooler (warmer) conditions over most of the southern half of the basin, with opposite sign anomalies elsewhere. The $WPWP^+$ ($WPWP^-$) phase is associated with wetter (drier) conditions over essentially the southern half of the basin, with opposite sign anomalies elsewhere. Temperatures are generally higher in the basin under $WPWP^+$ and lower under $WPWP^-$.

b. Impacts on total and groundwater yields

Impacts of various DCV scenarios were evaluated by defining total water yield (referred to as water yield hereafter), as the net amount of water that leaves each

TABLE 3. Four-digit subbasin statistics (avg, std dev, and max positive and negative changes in each four-digit subbasin) of SWAT-simulated annual-average water yield (% change from climatology) in 29 subbasins in the MRB in PDO⁺ and PDO⁻ phases.

Subbasin	% Significant area	PDO ⁺				PDO ⁻			
		Avg	Std dev	Max	Min	Avg	Std dev	Max	Min
1002	39.95	1.06	1.68	7.63	-4.13	-0.76	1.68	5.73	-4.36
1003	13.80	0.38	3.29	15.57	-4.62	0.19	3.14	8.31	-13.99
1004	12.44	6.36	12.74	37.21	-20.33	-2.08	8.38	17.70	-20.40
1005	5.65	6.96	10.08	35.34	-10.58	-6.91	12.31	10.16	-37.12
1006	4.44	-1.19	9.09	24.72	-8.63	2.36	8.85	16.03	-22.15
1007	18.41	0.20	3.48	18.72	-6.58	-0.13	3.76	9.71	-19.05
1008	24.86	2.99	4.39	27.31	-3.65	-2.31	3.48	3.93	-28.16
1009	21.72	5.96	5.29	24.11	-7.60	-3.74	3.67	7.10	-17.09
1010	16.71	6.03	8.29	36.17	-6.20	-3.30	5.42	6.54	-14.54
1011	20.56	4.24	6.47	22.78	-14.14	-3.49	5.71	6.26	-22.05
1012	33.68	6.68	4.99	28.15	-5.16	-6.39	5.02	1.98	-41.09
1013	13.78	3.89	6.38	23.08	-16.83	-1.97	5.52	19.91	-14.04
1014	60.91	6.22	4.14	28.21	0.37	-5.96	4.02	0.34	-21.69
1015	66.58	6.54	5.81	37.05	-0.46	-6.12	4.61	0.94	-23.05
1016	37.09	5.36	3.56	22.17	0.65	-4.78	2.82	-0.50	-14.18
1017	76.40	7.12	3.50	19.26	1.09	-6.14	2.46	-0.91	-16.85
1018	28.81	3.63	4.11	24.81	-7.21	-3.36	3.65	5.09	-17.73
1019	38.13	5.89	6.61	30.43	-7.72	-5.25	5.74	7.52	-24.66
1020	94.26	6.50	4.23	26.11	0.32	-5.87	3.49	-0.54	-24.00
1021	83.91	6.87	5.56	27.80	0.18	-6.12	4.88	0.18	-21.98
1022	96.15	5.93	2.21	15.78	1.93	-5.75	2.16	-1.34	-13.39
1023	67.06	3.28	1.73	10.36	-1.62	-3.14	1.54	1.35	-8.10
1024	99.20	4.08	1.76	13.15	0.73	-4.12	1.61	-0.71	-9.50
1025	47.16	4.42	4.43	30.10	-1.05	-3.98	3.75	0.83	-19.35
1026	77.80	4.67	3.48	31.74	0.23	-4.62	3.02	0.06	-20.53
1027	96.99	7.31	6.28	39.71	-0.77	-6.42	4.81	-0.78	-39.17
1028	99.68	4.40	1.57	9.91	0.63	-4.64	1.74	-0.60	-10.36
1029	100.00	4.65	1.68	10.71	1.11	-4.45	1.59	-1.16	-10.23
1030	100.00	5.05	2.05	16.18	0.98	-4.89	1.90	-0.78	-12.30

12-digit subbasin and contributes to flow in the nearest stream/river. The groundwater contribution (referred to as groundwater hereafter) to the total water yield was defined as the water from the shallow aquifer that returns to the nearest stream/river. Simulation results of IDS-Avg scenarios are described in this section. Simulation results were displayed in a variety of formats—two-dimensional (longitude–latitude) figures, histograms aggregated over a part or all of the MRB, and tables of statistics of water yield changes—for each DCV scenario. In the twin interests of clarity and brevity, only selected examples are shown in this paper.

IDS-Avg water yield (Fig. 4a) increased by 10%–30% of average yield in most of the MRB in response to forcing anomalies associated with PDO⁺ (Figs. 1a,c), but not in eastern and western Montana, western North Dakota, and individual locations in South Dakota, Nebraska, Colorado, and Wyoming, where the yield decreased by 10%–20%. In response to forcing anomalies associated with PDO⁻ (Figs. 1b,d), water yield (Fig. 4b) decreased almost everywhere by 10%–20%, except for

some isolated locations in Montana, North and South Dakota, Wyoming, Colorado, and Nebraska. The average water yield change over the entire MRB in both phases of the PDO was within $\pm 20\%$ of average yield.

As Fig. 4 shows, the response of water yield to the two PDO scenarios at the 12 km \times 12 km resolution is rich in detail and quite varied over the entire MRB in the magnitude of the changes. Therefore, in order to quantify and assess the response in larger subbasins, the high-resolution changes were aggregated in four-digit subbasins identified by USGS.

A map of 29 of the 30 four-digit subbasins in the MRB is shown in Fig. 5. Spatial average and standard deviation of water yield changes in each four-digit subbasin, maximum and minimum values of changes in each subbasin, and the percent of each subbasin's area in which changes are statistically significant were calculated and tabulated for each DCV scenario. Table 3 shows the calculated statistics for PDO⁺ and PDO⁻ scenarios in each four-digit subbasin. The table shows several interesting attributes of the water yield response to the two PDO scenarios. Generally, there is a

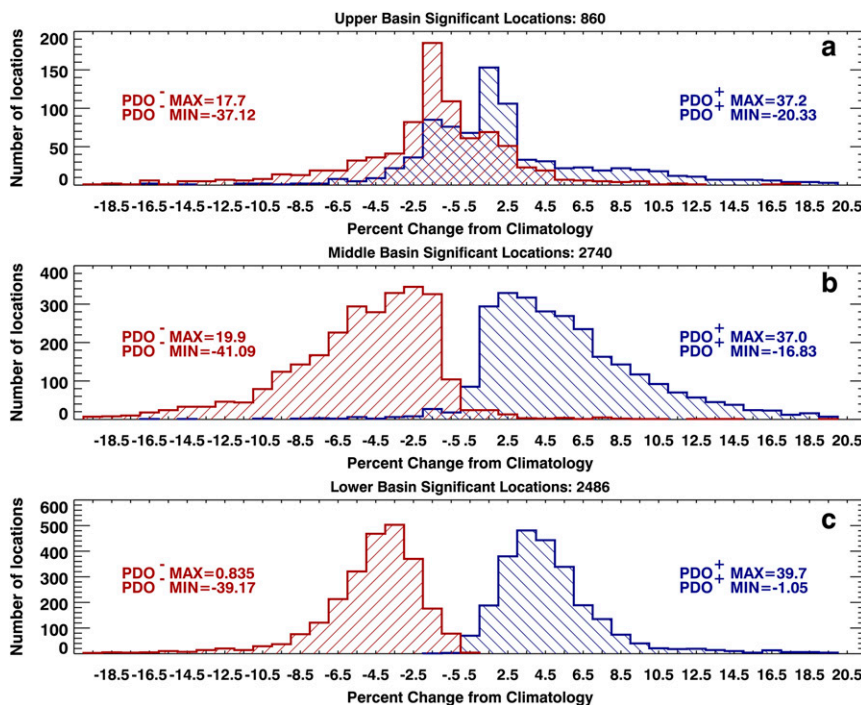


FIG. 6. Histograms of aggregated water yields in three parts of the MRB for PDO^+ and PDO^- : (a) upper, (b) middle, and (c) lower.

progression of large-scale increases in DCV impacts—as characterized by percent area with significant changes—from the upper part of the MRB (subbasins 1002–1013) to the middle part (subbasins 1014–1023) to the lower part (subbasins 1024–1030). The table also shows generally more homogeneous changes within a subbasin—as characterized by the spatial standard deviation—from the upper part (larger standard deviation) to the middle and lower parts (smaller standard deviation). The table also shows an increasing distinctness of the response to PDO^+ and PDO^- scenarios—as characterized by decreasing overlap of the range of changes within each subbasin—from the upper part (more overlap in range) to the middle part (less overlap in range) to the lower part (very little overlap in range).

The water yield changes for PDO^+ and PDO^- , evident in Fig. 4 and Table 3, were further aggregated in histograms for each of the three major parts of the MRB. These histograms aggregated water yield changes in bins at all locations that have statistically significant yield changes. These histograms are shown in Fig. 6. Because of small numbers of locations in all distributions at yield change magnitudes larger than 20%, the x-axis range is restricted to values from -20.5% to 20.5% in Fig. 6; the maximum and minimum values of yield changes in each part of the MRB are given in Fig. 6. Following Mehta

et al. (2011), a test of significance of differences in the binned distributions corresponding to positive and negative phases of each DCV phenomenon was conducted (Press et al. 2007). This test showed that, for all three DCV phenomena, the probabilities of the distributions corresponding to positive and negative phases belonging to the same population were smaller than 10^{-12} , implying that impacts of positive and negative phases of each DCV phenomenon were significantly different. In Fig. 6, as seen in Table 3, the number of locations where changes are significant increases and the overlap between changes in PDO^+ and PDO^- decreases from the upper to the lower part of the MRB. The histograms clearly show that PDO^+ and PDO^- scenarios substantially and significantly impact water yields to varying degrees in the three parts of the MRB. Histograms aggregated over the entire MRB for each of the two PDO scenarios (not shown) indicate a net impact on water yields with the range of changes in PDO^+ from -20% to 39% and in PDO^- from -41% to 20% in 6086 locations (45% of the total number of locations where the SWAT experiments were run) where the changes are significant. The net change in water yield in the MRB is approximately 15% between the two PDO phases.

Although water yield in individual watersheds is an important variable for water resources and agriculture,

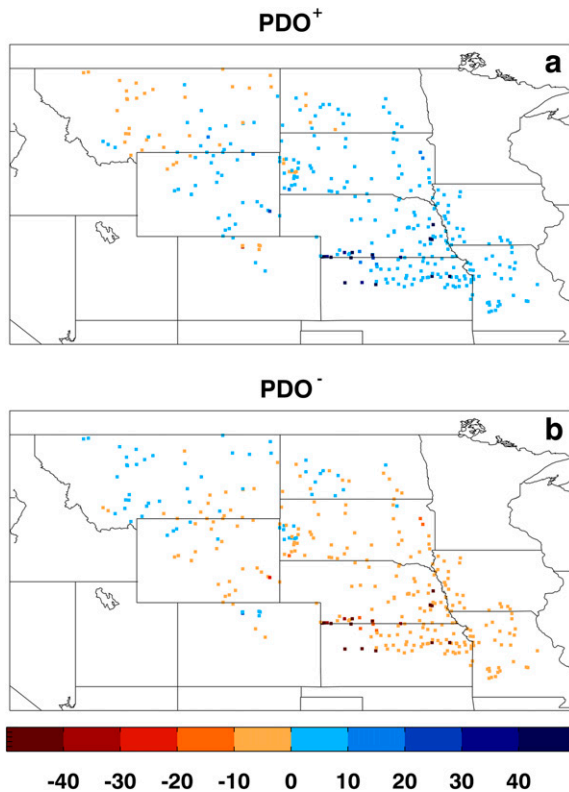


FIG. 7. Ratio (%) of SWAT-simulated streamflow anomalies and 30-yr (1981–2010) average streamflows measured by the USGS gauges: (a) PDO^+ and (b) PDO^- .

it is a SWAT-specific variable. So, in order to assess the “real world” importance of SWAT-simulated impacts of DCV phenomena, these results are compared with observations. The ratio of SWAT-simulated streamflow anomalies in the two PDO scenarios and 30-yr (1981–2010) average of streamflow measured by USGS gauges was calculated where the latter data are available in the MRB (Fig. 7). The SWAT-simulated streamflow anomalies are generally in the $\pm 20\%$ range, with a few locations in Nebraska and Kansas exceeding this range. Figure 7 also shows the generally opposite signs of SWAT-simulated streamflow anomalies in the two PDO scenarios. Thus, it is clear that SWAT-simulated impacts of the two PDO scenarios in the MRB are substantial when compared to long-term averages of gauge-measured streamflows.

In response to forcing anomalies associated with the two TAG scenarios, the water yield responses were much less homogeneous spatially, especially in the upper part of the MRB, compared to the responses to the two PDO scenarios; this is evident in the original high-resolution figures (not shown) as well as in the table of statistics (not shown) in each four-digit subbasin.

Generally, there was antisymmetry in the signs of water yield anomalies between TAG^+ and TAG^- . In the interest of brevity, only the histograms aggregated in each of the three parts of the MRB are shown here in Fig. 8. Overlaps in ranges of water yield changes and frequency distributions are evident in the upper part of the MRB in Fig. 8a. These overlaps decrease in the middle and lower parts of the MRB. Histograms aggregated over the entire MRB for each of the two TAG scenarios (not shown) indicate a net impact on water yields with the range of changes in TAG^+ from -44% to 28% and in TAG^- from -26% to 45% in 3529 locations (26% of the total number of locations where the SWAT experiments were run) where the changes are significant. The net change in water yield in the MRB is approximately 5%–10% between the two TAG phases. Overall, including in histograms aggregated in the entire MRB for the two TAG scenarios, it appears that responses to the two TAG scenarios reflect inhomogeneities in hydro-meteorological anomalies associated with these two scenarios (Fig. 2) and more pronounced effects of local conditions.

Water yield responses to the two WPWP scenarios are also inhomogeneous as evident in the original high-resolution figures (not shown) and the table of four-digit subbasin statistics (not shown). As discussed earlier in this section, there were below-average precipitation and above-average temperatures in $WPWP^+$, generally resulting in below-average water yield in almost the entire MRB. The opposite situation prevailed in $WPWP^-$. Although there are substantially large (up to 30% or more) changes in water yield at individual locations in the two WPWP scenarios, the changes aggregated in upper, middle, and lower parts of the MRB are usually $\pm 5\%$ of climatological water yields, as is evident in the histograms in Fig. 9. Also, in the middle part of the MRB, there are substantial overlaps in ranges of changes in the two WPWP scenarios. Histograms aggregated over the entire MRB for each of the two WPWP scenarios (not shown) indicate a net impact on water yields with the range of changes in $WPWP^+$ from -31% to 13% and in $WPWP^-$ from -20% to 32% in 4020 locations (30% of the total number of locations where the SWAT experiments were run) where the changes are significant. The net change in water yield in the MRB is approximately less than 5% between the two WPWP phases.

To summarize the findings displayed and described above, there were significant and large impacts of PDO phases on surface water in the southern half of the basin and isolated, smaller spatial-scale impacts in the northern half. There was generally 30% or more surface water under PDO^+ and 20%–30% less under

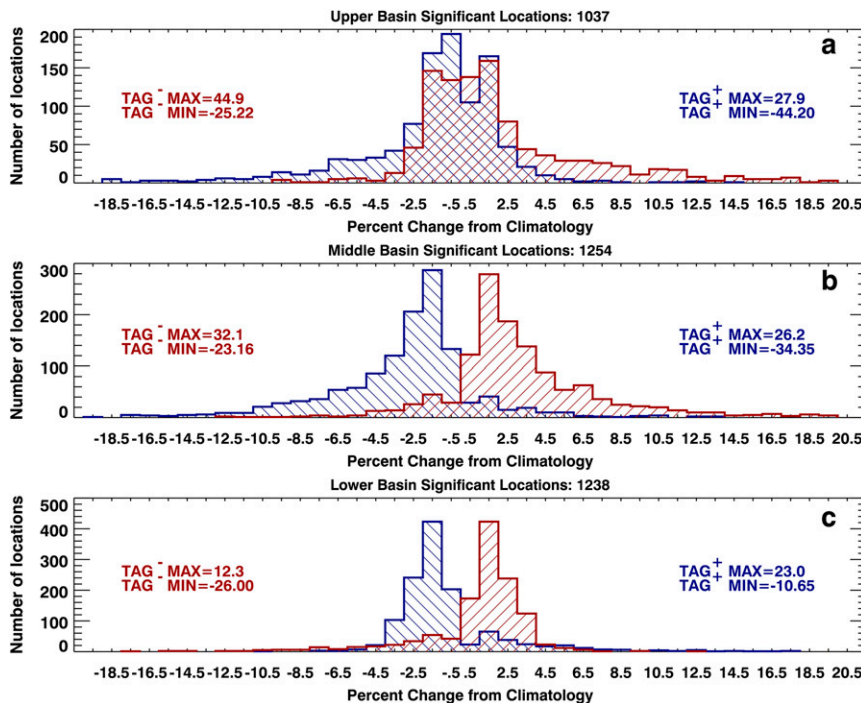


FIG. 8. Histograms of aggregated water yields in three parts of the MRB for TAG⁺ and TAG⁻: (a) upper, (b) middle, and (c) lower.

PDO⁻. In TAG phases, there were generally the same sign of surface water anomalies in the basin, except in a swath from west-central Kansas to southeastern Nebraska–northwestern Missouri, western Montana, and the North and South Dakota border. Surface water anomalies were of the same sign in PDO⁺ and TAG⁻; this is also true for PDO⁻ and TAG⁺. There are small ($\pm 10\%$) surface water anomalies associated with WPWP phases, generally of the same signs as under TAG⁺ and TAG⁻.

The forcing anomalies associated with each phase of the three DCV phenomena persist for several years, recharging underground water, some of which flows into streams and rivers. The quantity of lateral groundwater flow depends on areal extent and magnitude of forcing anomalies, soil characteristics, and topography. The SWAT experiments showed, however, that the latter two factors dominate the groundwater contribution to total water yields in the MRB and that the ratio of groundwater contribution to the total water yield is the same at any particular location in both the climatology and DCV scenario experiments.

The groundwater contributions to lateral flow (not shown) were 10%–20% of the total water yield in much of the MRB, except along the eastern boundary of the basin in South Dakota, eastern Nebraska, western Iowa,

and in central Missouri, where the groundwater contribution was as much as 30%. In a few small regions in eastern Montana, western and central North Dakota, northeastern South Dakota, eastern Nebraska, and northern Iowa, the groundwater contribution to water yield was 60%–80%.

5. Impacts of multiple decadal climate variability scenarios

a. Hydrometeorological anomalies associated with each scenario

In the second set of SWAT experiments, titled CDS-Avg, we studied the response of water yield to scenarios in which three DCV phenomena occurred simultaneously. All eight of the multiple-DCV scenarios (section 3c) affect hydrometeorology of the basin, with (PDO⁺, TAG⁻, WPWP^{+/-}) and (PDO⁻, TAG⁺, WPWP^{+/-}) combinations producing maximal impacts. The PDO⁺ and TAG⁻ phases occurring together produced generally wetter and cooler conditions, whereas the PDO⁻ and TAG⁺ phases reinforced one another to produce generally drier and warmer conditions. As previously noted, WPWP phases generally have marginal effects on the overall basin hydrometeorology.

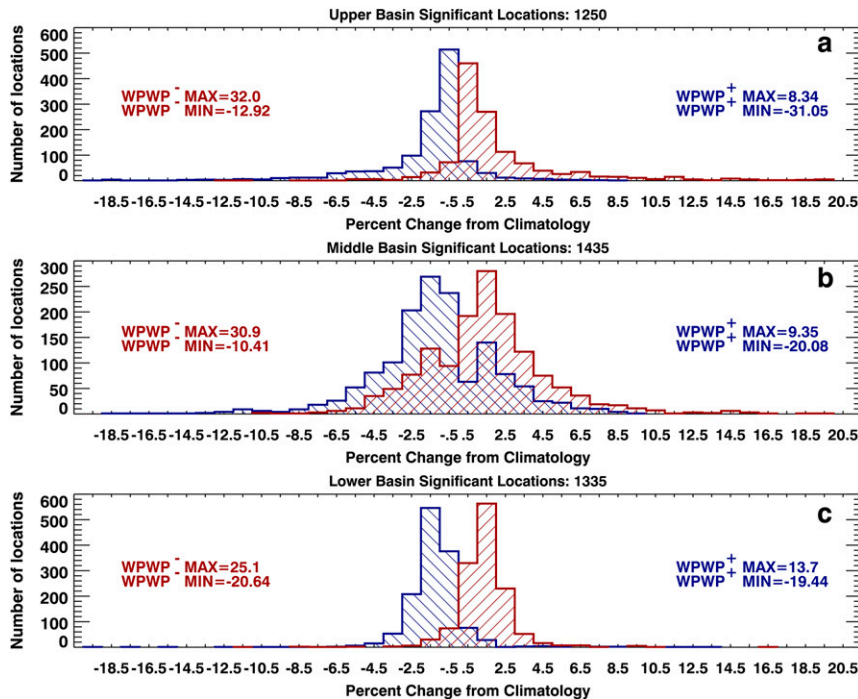


FIG. 9. Histograms of aggregated water yields in three parts of the MRB for $WPWP^+$ and $WPWP^-$: (a) upper, (b) middle, and (c) lower.

b. Impacts on total water yields

Since combinations of opposite phases of PDO and TAG produced maximal impacts, their effects in CDS-Avg scenarios on surface and groundwater are described here. As Fig. 10 shows, with WPWP in its positive phase, the impacts of the (PDO^+, TAG^-) and (PDO^-, TAG^+) scenarios on surface water were greater than those of either the PDO (Fig. 4) or the TAG (not shown) alone at most of the 13 500 locations where the impacts were simulated. In the former scenario with $WPWP^+$ (Fig. 10a), there were 30%–40% or even larger increases in water yield in the southeastern part of the MRB (eastern and central Nebraska, eastern Kansas, southwestern Iowa, and Missouri). There were also large increases in parts of South Dakota, central Montana, and southwestern Nebraska. There were small decreases ($\sim 10\%$), mostly in the northern part of the MRB and in relatively small and isolated areas in Wyoming, Nebraska, and Kansas. Overall, the increases were much greater in this CDS-Avg scenario than in IDS-Avg PDO^+ or TAG^- scenarios alone. In the (PDO^-, TAG^+) scenario with $WPWP^+$ (Fig. 10b), there was a 20%–30% or even larger decrease in water yield, generally in the same areas where large increases appear in Fig. 10a. This complementarity was due to superposition of positive anomalies in PDO^+ and TAG^- and

superposition of negative anomalies in PDO^- and TAG^+ . In both its phases, WPWP made substantial impacts on surface water in North and South Dakota, Montana, Nebraska, Kansas, and Missouri. Because of generally opposite signs of hydrometeorological anomalies, the (PDO^+, TAG^+) and (PDO^-, TAG^-) CDS-Avg scenarios reduced impacts on surface water of either phenomenon or phase alone.

These changes at individual locations in Fig. 10 were aggregated in upper, middle, and lower parts of the MRB and are shown in Fig. 11. They show mixed-sign responses and also the large ranges of water yield changes in the upper part of the MRB. They also show that the responses for the two 3-DCV combinations are much more separated and homogeneous in the middle and lower parts of the basin.

6. Impacts of extreme magnitudes of decadal climate variability phenomena

The results described in the preceding two sections were obtained with idealized single-DCV (IDS-Avg) and multiple-DCV (CDS-Avg) scenarios using average magnitudes of DCV indices observed over the 1949–2010 period. SWAT runs were also made with DCV scenarios encompassing extreme magnitudes of PDO, TAG, and WPWP indices observed during the

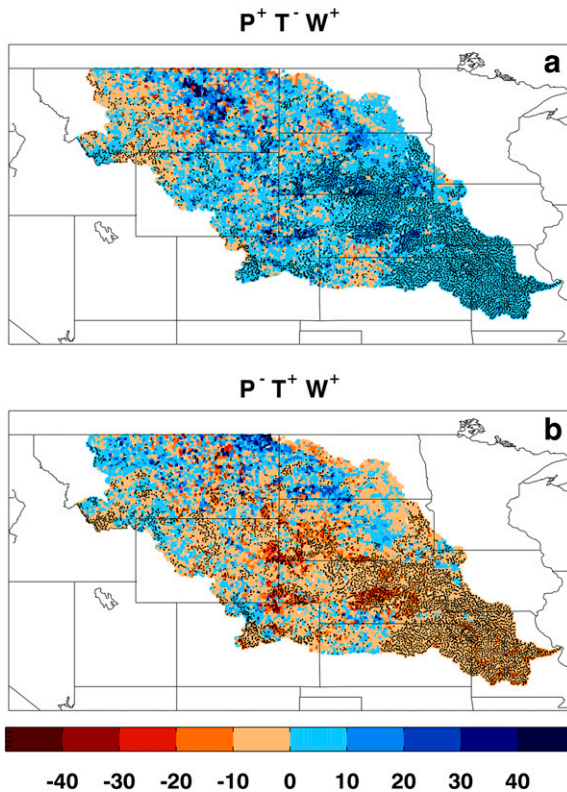


FIG. 10. SWAT-simulated annual-average water yield (% change from climatology) in the MRB in (a) $(PDO^+, TAG^-, WPWP^+)$ and (b) $(PDO^-, TAG^+, WPWP^+)$ scenarios. Black dots show locations of 95% significance.

1949–2010 period; these scenarios are referred to as IDS-Extremes and CDS-Extremes, as described in section 3c. Results of these SWAT experiments are described in this section.

In single-DCV scenarios with extreme magnitudes (IDS-Extremes), the spatial distribution of impacts on water yield were generally the same as appears in the average magnitude single-DCV scenarios (IDS-Avg) discussed in section 4b. Water yields in the IDS-Extremes scenarios increased by approximately 10%–20% (not shown). In multiple DCV scenarios (CDS-Extremes), however, the impacts of extreme DCV magnitudes were magnified by superposition of same-sign anomalies. Again, (PDO^+, TAG^-) and (PDO^-, TAG^+) scenarios, coupled with the same WPWP phases, led to maximal impacts on water yields. MRB-aggregated histograms in Fig. 12 show percent change in water yield in the $(PDO^+, TAG^-, WPWP^+)$ and $(PDO^-, TAG^+, WPWP^+)$ CDS-Extremes scenarios, respectively. Note that the percent change scale in Fig. 12 spans twice as large a range as in corresponding average magnitude results shown in Fig. 11. Thus, these results show that extreme magnitudes and opposite

phases of PDO and TAG can cause devastating droughts and wet periods in the MRB.

7. Discussion and conclusions

We conducted experiments with an advanced high-resolution version of SWAT, calibrated and validated for the MRB to estimate impacts of the PDO, TAG, and WPWP on surface and groundwater flows in the basin. Impacts of positive and negative phases of individual DCV phenomena as well as of combinations of the three DCV phenomena were simulated by forcing SWAT at approximately 13 500 locations (approximate grid spacing of $12\text{ km} \times 12\text{ km}$, latitude–longitude) with idealized hydrometeorological scenarios associated with the DCV phenomena. Experiments were conducted with average magnitudes and with extreme magnitudes of the three DCV phenomena as observed from 1949 to 2010. Major results of this study are as follows:

- All six individual DCV scenarios (three DCV phenomena \times two phases each) affect hydrometeorology of the MRB, with the most substantial impacts from PDO followed by TAG and WPWP.
- All eight multiple-DCV scenarios affect hydrometeorology of the basin, with $(PDO^+, TAG^-, WPWP^{+/-})$ and $(PDO^-, TAG^+, WPWP^{+/-})$ scenarios producing maximal impacts.
- There are significant impacts on surface water over the entire basin, but only in its southeastern and northern parts is the groundwater contribution to surface flows noteworthy.
- Impacts of (PDO^+, TAG^-) and (PDO^-, TAG^+) combinations on surface water and groundwater are stronger (up to 30%–40% with respect to recent climatology) than of either of these DCV phenomena alone.
- Local conditions in the central and northern parts of the basin appear to influence responses to DCV phenomena more than in other parts of the basin.
- The above-mentioned impacts on hydrometeorology, surface water, and groundwater occur even under average magnitudes of the three DCV phenomena observed over the 1949–2010 period.
- Extreme magnitudes of the three DCV phenomena, acting individually or in concert, are associated with severe to extreme droughts and wet periods in the MRB.

These results clearly show that water yields are sensitive to changes in the forcings associated with individual phenomena and their phases. This is so since the hydrologic cycle is driven by precipitation and evapotranspiration, and the latter is determined by ambient

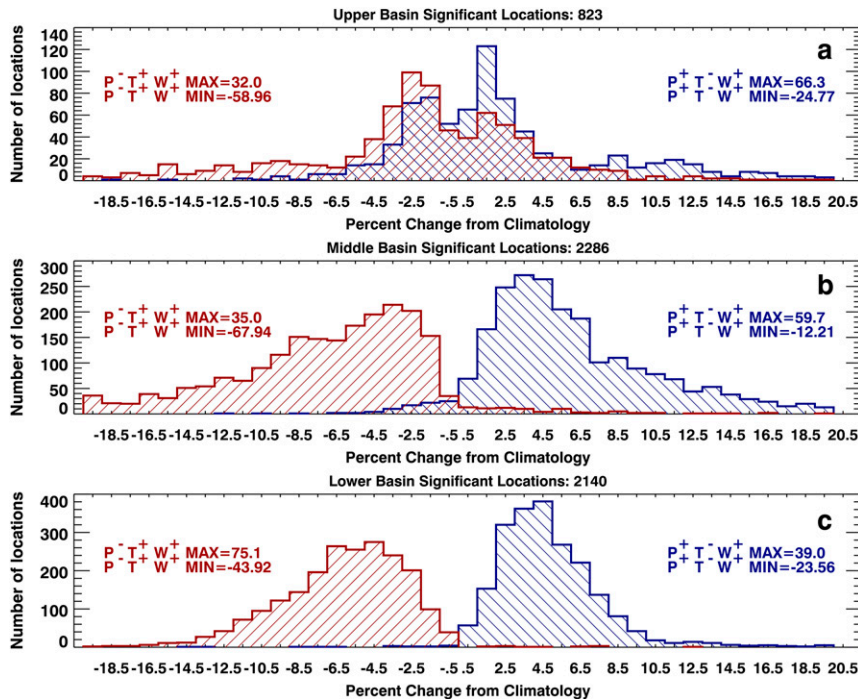


FIG. 11. Histograms of aggregated water yields in three parts of the MRB for $(\text{PDO}^+, \text{TAG}^-, \text{WPWP}^+)$ and $(\text{PDO}^-, \text{TAG}^+, \text{WPWP}^+)$ scenarios at average amplitudes: (a) upper, (b) middle, and (c) lower.

temperature and humidity and by windiness. To further relate results of simulations of idealized scenarios to occurrences of actual (or real world) dry and wet periods, we compared SWAT's responses to hydrometeorological anomalies associated with idealized DCV scenarios with observed streamflow at many locations in the MRB, and also simulations of observed, persistent dry, and persistent wet periods by SWAT. The empirical association between maxima and minima in observed streamflows and phases of PDO and TAG is similar to the implications of the simulation results from this study.

To further compare impacts of idealized DCV scenarios and observed streamflows, we simulated annual-average daily streamflow in one wet (1982–86) and one dry (1987–90) period in the MRB. The PDO index was in positive phase during the wet period and negative phase during much of the dry period. The TAG index was in negative phase during the wet period, but fluctuated between positive and negative phases during the dry period. For these time periods, SWAT was forced by observed, daily hydrometeorological anomalies from Maurer et al. (2002) at each of the approximately 13 500 locations. The observed and simulated streamflow anomalies, calculated with respect to corresponding climatology, for the wet and dry periods are shown in Figs. 13 and 14, respectively. Annual-average daily

streamflow anomalies at specific locations observed by the USGS gauge network in the MRB and simulated by SWAT at the same locations are generally similar for the 1982–86 wet period and the 1987–90 dry period as Figs. 13a, 13b, 14a, and 14b show. Differences between the observed and simulated streamflow anomalies are reasonably small, as Figs. 13c and 14c show. A scatterplot of observed versus simulated streamflow anomalies, the data shown in these two figures, shows that an overwhelming number of data points within $\pm 40 \text{ m}^3 \text{ s}^{-1}$ lay along the slope = 1 line, implying that SWAT simulates the observed flow anomalies in this range very well. At observed flow anomalies below average by $60 \text{ m}^3 \text{ s}^{-1}$ and larger, SWAT underestimates the flows, and at observed flow anomalies $35\text{--}40 \text{ m}^3 \text{ s}^{-1}$, SWAT overestimates the flows. Thus, the simulated impacts of DCV phenomena appear to be consistent with observed association between DCV phenomena and streamflow anomalies in the MRB. Perfect agreement should not be expected, however, as topography, soil type, antecedent soil moisture conditions, and vegetative cover are also controlling surface and groundwater flows, and all of the latter factors were treated as uniform over the entire area of each 12-digit subbasin. Although outliers exist, SWAT-simulated water yields and streamflows were generally consistent with DCV anomalies in forcings, both locally and regionally in this study.

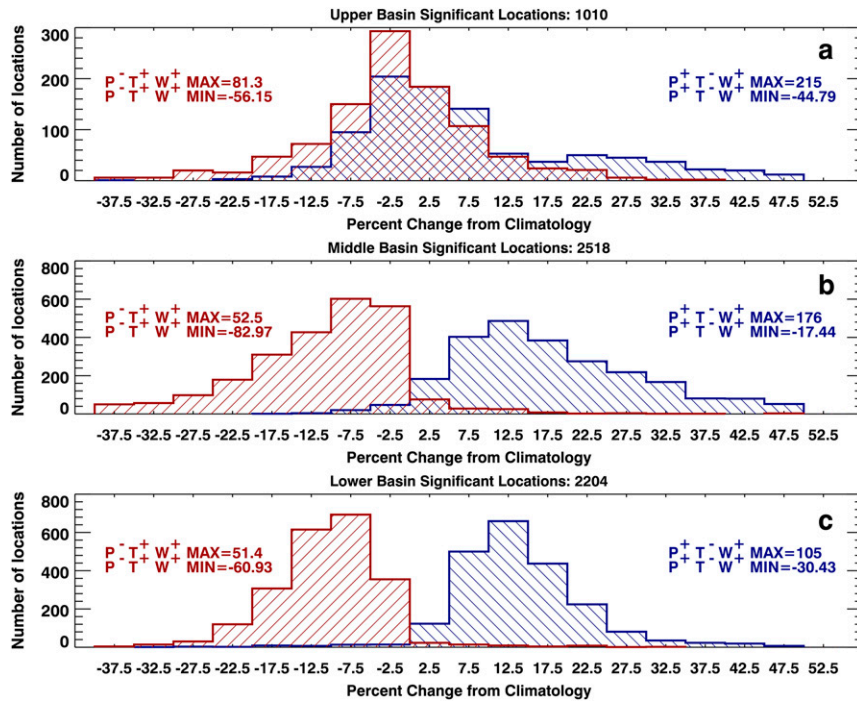


FIG. 12. Histograms of aggregated water yields in three parts of the MRB for $(PDO^+, TAG^-, WPWP^+)$ and $(PDO^-, TAG^+, WPWP^+)$ scenarios at extreme amplitudes: (a) upper, (b) middle, and (c) lower.

A comparison of simulated impacts of idealized DCV scenarios on water yields—described in this paper—with our exploratory study (Mehta et al. 2011) shows that while the overall spatial patterns of impacts of individual DCV phenomena on water yields in the MRB are generally similar, impacts are much larger in magnitude at some locations and in some four-digit basins in the present study. This difference may be largely due to the much higher resolution employed in the present study and also due to the meticulous calibration and validation of the very high-resolution SWAT employed in this study. There are 180 times more samples in the present study (~13 500 locations), so analyses results are much more accurate and reliable compared to the exploratory study where there were only 75 locations in the entire MRB. Another major difference is that the exploratory study did not simulate impacts of multiple, simultaneous DCV phenomena on water yields. As shown by this study, impacts of (PDO^+, TAG^-) and (PDO^-, TAG^+) combinations can be much larger in magnitude than those of an individual DCV phenomenon at its average amplitude, the former combination potentially causing major and long-lasting wet spells and the latter severe to extreme droughts. These implications of the present study about extreme hydrologic impacts of decadal anomalies in Pacific and Atlantic

SSTs are consistent with results of atmospheric general circulation model experiments by Schubert et al. (2009). Of course, the biggest difference between the present and exploratory studies is the usability of the present results by stakeholders and policymakers as explained in section 2.

With reference to the three questions posed in this study (section 2), we found that there are substantial impacts of the three DCV phenomena at their average magnitudes on surface and groundwater and on streamflows in the MRB (question 1). We also found that combinations of opposite phases of PDO and TAG can create dry and wet conditions in the MRB, much more severe than either individual phenomenon alone (question 2). These impacts are even more severe when the DCV phenomena have extreme magnitudes, creating extreme and long-lasting hydrologic events such as severe to extreme droughts and wet periods (question 3). We also found that soil characteristics and topography dominate groundwater contributions to lateral flow in the climatological and DCV scenario experiments. The groundwater contributions to lateral flow were small but significant in much of the MRB, except along the eastern boundary of the basin in South Dakota, eastern Nebraska, western Iowa, and in central Missouri. In a few small regions in eastern Montana, western and central

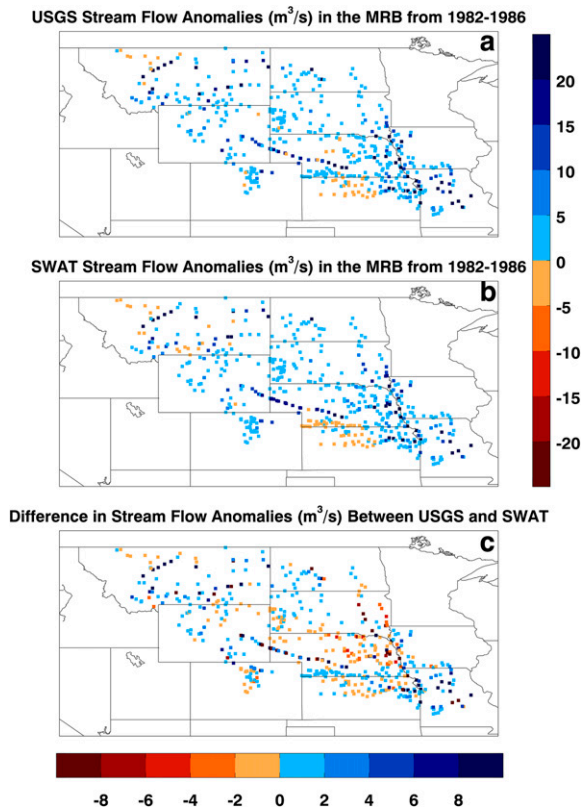


FIG. 13. Annual-average streamflow ($\text{m}^3 \text{s}^{-1}$) in the MRB from 1982 to 1986: (a) observed USGS estimate, (b) simulated SWAT estimate, and (c) difference between (a) and (b).

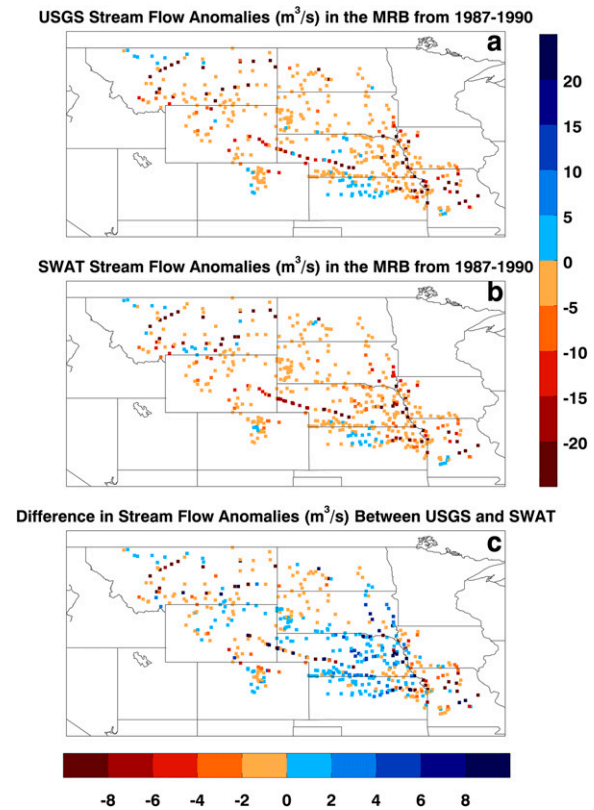


FIG. 14. Annual-average streamflow ($\text{m}^3 \text{s}^{-1}$) in the MRB from 1987 to 1990: (a) observed USGS estimate, (b) simulated SWAT estimate, and (c) difference between (a) and (b).

North Dakota, northeastern South Dakota, eastern Nebraska, and northern Iowa, the groundwater contribution was much larger. Thus, this study has provided conclusive and insightful answers to the three major questions.

Our results show that, if they occur individually, the three DCV phenomena considered in this study can significantly impact water yields and streamflows in the MRB. As these DCV phenomena can persist in one phase or the other for a few years to a decade or longer, and as the simultaneous correlation among them is negligibly small, their combined and cumulative effects on the MRB hydrometeorology should be sufficient to impact all water sectors in the region—nonirrigated and irrigated agriculture, municipal and industrial needs, transportation, hydropower generation, fish and wildlife habitat, and recreation. These results also imply important consequences of these impacts on water yields to feedbacks to the climate system via water vapor and heat fluxes.

The MRB is a major “breadbasket” in which most food and feed crops are produced on nonirrigated land. In periods of drought, agricultural production is reduced and the contribution of irrigated land to regional

production can also be significantly curtailed by shortages in surface water supply. In periods of ample rainfall, the overall contribution of irrigation to regional production is, of course, less critical. Because the three DCV phenomena whose impacts on water yields were modeled in this study are known to influence climate and hydrometeorology in other parts of the world also (as do other DCV phenomena not addressed in this study), our methodology should be applicable to such regions as well. It is certainly possible that in the foreseeable future the evolution of major DCV phenomena will be forecast with useable skill. If so, it may become possible, with SWAT and other well-validated hydrology models, to forecast multiyear to decadal impacts of the DCV phenomena on water yields and streamflows in those regions known to be affected by the phenomena. We are working toward that goal with experimental decadal climate and impacts predictions and further improvements in SWAT as outlined in the introduction.

Acknowledgments. This research was supported by the U.S. Department of Agriculture National Institute of Food and Agriculture under Grant 2011-67003-30213 in

the NSF–USDA–DOE Earth System Modeling Program and by the NOAA/Climate Program Office Sectoral Applications Research Program Grant NA12OAR4310097. The authors are grateful to three anonymous reviewers and to Andrew Wood, the Editor, for their comments and suggestions on an earlier version of this paper.

REFERENCES

- Abbaspour, K. C., M. Vejdani, and S. Haghghat, 2007: SWAT-CUP calibration and uncertainty programs for SWAT. *MODSIM 2007 International Congress on Modelling and Simulation*, L. Oxley and D. Kulasiri, Eds., Modelling and Simulation Society of Australia and New Zealand, 1596–1602. [Available online at http://www.mssanz.org.au/MODSIM07/papers/24_s17/SWAT-CUP_s17_Abbaspour_.pdf.]
- An, S.-I., and B. Wang, 2000: Interdecadal change of the structure of the ENSO mode and its impact on the ENSO frequency. *J. Climate*, **13**, 2044–2055, doi:10.1175/1520-0442(2000)013<2044:ICOTSO>2.0.CO;2.
- Arnold, J. G., and P. M. Allen, 1993: A comprehensive surface–groundwater flow model. *J. Hydrol.*, **142**, 47–69, doi:10.1016/0022-1694(93)90004-S.
- , R. Srinivasan, R. S. Muttiah, and P. M. Allen, 1999: Continental scale simulation of the hydrologic balance. *J. Amer. Water Resour. Assoc.*, **35**, 1037–1051, doi:10.1111/j.1752-1688.1999.tb04192.x.
- Balmaseda, M. A., M. K. Davey, and D. L. T. Anderson, 1995: Decadal and seasonal dependence of ENSO prediction skill. *J. Climate*, **8**, 2705–2715, doi:10.1175/1520-0442(1995)008<2705:DASDOE>2.0.CO;2.
- Cayan, D. R., M. D. Dettinger, H. F. Diaz, and N. E. Graham, 1998: Decadal variability of precipitation over western North America. *J. Climate*, **11**, 3148–3166, doi:10.1175/1520-0442(1998)011<3148:DVOPOW>2.0.CO;2.
- Chang, P., L. Ji, and H. Li, 1997: A decadal climate variation in the tropical Atlantic Ocean from thermodynamics and air–sea interactions. *Nature*, **385**, 516–518, doi:10.1038/385516a0.
- Cooke, M., and Coauthors, 1936: Report of the Great Plains Drought Area Committee. Report to President Franklin D. Roosevelt, Franklin D. Roosevelt Library, Hopkins Papers, Box 13. [Available online at <http://newdeal.feri.org/Texts/450.htm>.]
- Cooley, H., N. Ajami, M.-L. Ha, V. Srinivasan, J. Morrison, K. Donnelly, and J. Christian-Smith, 2013: Global water governance in the 21st century. Pacific Institute, Oakland, CA, 34 pp. [Available online at <http://www.pacinst.org/publication/global-water-governance-in-the-21st-century-2/>.]
- Dagupati, P., D. Deb, R. Srinivasan, D. Yeganantham, V. M. Mehta, and N. J. Rosenberg, 2016: Large-scale fine-resolution hydrological modeling using parameter regionalization in the Missouri River basin. *J. Amer. Water Resour. Assoc.*, **52**, 648–666, doi:10.1111/1752-1688.12413.
- Di Luzio, M., R. Srinivasan, and J. G. Arnold, 2002: Integration of watershed tools and SWAT model into BASINS. *J. Amer. Water Resour. Assoc.*, **38**, 1127–1141, doi:10.1111/j.1752-1688.2002.tb05551.x.
- Enfield, D. B., A. M. Mestas, D. A. Mayer, and L. Cid-Serrano, 1999: How ubiquitous is the dipole relationship in tropical Atlantic sea surface temperatures? *J. Geophys. Res.*, **104**, 7841–7848, doi:10.1029/1998JC900109.
- Gassman, P. W., A. M. Sadeghi, and R. Srinivasan, 2014: Applications of the SWAT model special section: Overview and insights. *J. Environ. Qual.*, **43**, 1–8, doi:10.2134/jeq2013.11.0466.
- Gleick, P. H., 1993: Water and conflict: Fresh water resources and international security. *Int. Secur.*, **18**, 79–112, doi:10.2307/2539033.
- Guetter, A. K., and K. P. Georgakakos, 1993: River outflow of the conterminous United States. *Bull. Amer. Meteor. Soc.*, **74**, 1873–1891, doi:10.1175/1520-0477(1993)074<1873:ROOTCU>2.0.CO;2.
- Gurdak, J. J., R. T. Hanson, P. B. McMahon, B. W. Bruce, J. E. McCray, G. D. Thyne, and R. C. Reedy, 2007: Climate variability controls on unsaturated water and chemical movement, High Plains Aquifer, USA. *Vadose Zone J.*, **6**, 533–547, doi:10.2136/vzj2006.0087.
- Hidalgo, H. G., 2004: Climate precursors of multidecadal drought variability in the western United States. *Water Resour. Res.*, **40**, W12504, doi:10.1029/2004WR003350.
- Houghton, R. W., and Y. Tourre, 1992: Characteristics of low-frequency sea surface temperature fluctuations in the tropical Atlantic. *J. Climate*, **5**, 765–771, doi:10.1175/1520-0442(1992)005<0765:COLFSS>2.0.CO;2.
- Jayakrishnan, R., R. Srinivasan, C. Santhi, and J. G. Arnold, 2005: Advances in the application of the SWAT model for water resources management. *Hydrol. Processes*, **19**, 749–762, doi:10.1002/hyp.5624.
- Kannan, N., C. Santhi, M. Di Luzio, S. Potter, and J. G. Arnold, 2005: Measuring environmental benefits of conservation practices: The Conservation Effects Assessment Project (CEAP)—A model calibration approach at the national level. *2005 ASAE Annual Int. Meeting*, Tampa, FL, ASAE, 052131. [Available online at <http://naldc.nal.usda.gov/catalog/29003>.]
- , S. Chinnasamy, M. White, X. Wang, J. Arnold, and M. Di Luzio, 2011: Documentation on calibration and validation of CEAP-HUMUS for various river basins in the United States. USDA Doc., 169 pp. [Available online at http://www.nrcs.usda.gov/Internet/FSE_DOCUMENTS/stelprdb1044544.pdf.]
- Kestin, T. S., D. J. Karoly, and J.-I. Yano, 1998: Time-frequency variability of ENSO and stochastic simulations. *J. Climate*, **11**, 2258–2272, doi:10.1175/1520-0442(1998)011<2258:TFVOEA>2.0.CO;2.
- Lins, H. F., 1997: Regional streamflow regimes and hydroclimatology of the United States. *Water Resour. Res.*, **33**, 1655–1667, doi:10.1029/97WR00615.
- Mantua, N. J., S. R. Hare, Y. Zhang, J. M. Wallace, and R. C. Francis, 1997: A Pacific decadal climate oscillation with impacts on salmon. *Bull. Amer. Meteor. Soc.*, **78**, 1069–1079, doi:10.1175/1520-0477(1997)078<1069:APICOW>2.0.CO;2.
- Maurer, E. P., A. W. Wood, J. C. Adam, and D. P. Lettenmaier, 2002: A long-term hydrologically based dataset of land surface fluxes and states for the conterminous United States. *J. Climate*, **15**, 3237–3251, doi:10.1175/1520-0442(2002)015<3237:ALTHBD>2.0.CO;2.
- McCabe, G. J., M. A. Palecki, and J. L. Betancourt, 2004: Pacific and Atlantic Ocean influences on multidecadal drought frequency in the United States. *Proc. Natl. Acad. Sci. USA*, **101**, 4136–4141, doi:10.1073/pnas.0306738101.
- Meehl, G. A., and A. Hu, 2006: Megadroughts in the Indian monsoon region and southwest North America and a mechanism for associated multi-decadal Pacific sea surface temperature anomalies. *J. Climate*, **19**, 1605–1623, doi:10.1175/JCLI3675.1.
- , and Coauthors, 2009: Decadal prediction: Can it be skillful? *Bull. Amer. Meteor. Soc.*, **90**, 1467, doi:10.1175/2009BAMS2778.1.
- Mehta, V. M., 1998: Variability of the tropical ocean surface temperatures at decadal–multidecadal timescales. Part I: The Atlantic Ocean. *J. Climate*, **11**, 2351–2375, doi:10.1175/1520-0442(1998)011<2351:VOTTOS>2.0.CO;2.

- , and T. Delworth, 1995: Decadal variability of the tropical Atlantic Ocean surface temperature in shipboard measurements and in a global ocean–atmosphere model. *J. Climate*, **8**, 172–190, doi:10.1175/1520-0442(1995)008<0172:DVOTTA>2.0.CO;2.
- , N. J. Rosenberg, and K. Mendoza, 2011: Simulated impacts of three decadal climate variability phenomena on water yields in the Missouri River basin. *J. Amer. Water Resour. Assoc.*, **47**, 126–135, doi:10.1111/j.1752-1688.2010.00496.x.
- , —, and —, 2012: Simulated impacts of three decadal climate variability phenomena on dryland corn and wheat yields in the Missouri River basin. *Agric. For. Meteorol.*, **152**, 109–124, doi:10.1016/j.agrformet.2011.09.011.
- , C. L. Knutson, N. J. Rosenberg, J. R. Olsen, N. A. Wall, T. K. Bernadt, and M. J. Hayes, 2013a: Decadal climate information needs of stakeholders for decision support in water and agriculture production sectors: A case study in the Missouri River basin. *Wea. Climate Soc.*, **5**, 27–42, doi:10.1175/WCAS-D-11-00063.1.
- , H. Wang, and K. Mendoza, 2013b: Decadal predictability of tropical basin-average and global-average sea-surface temperatures in CMIP5 experiments with the HadCM3, GFDL-CM2.1, NCAR-CCSM4, and MIROC5 global earth system models. *Geophys. Res. Lett.*, **40**, 2807–2812, doi:10.1002/grl.50236.
- , —, —, and N. J. Rosenberg, 2014: Predictability and prediction of decadal hydrologic cycles: A case study in southern Africa. *Wea. Climate Extremes*, **3**, 47–53, doi:10.1016/j.wace.2014.04.002.
- Moriasi, D. N., J. G. Arnold, M. W. Van Liew, R. L. Binger, R. D. Harmel, and T. Veith, 2007: Model evaluation guidelines for systematic quantification of accuracy in watershed simulations. *Trans. ASABE*, **50**, 885–900, doi:10.13031/2013.23153.
- Murphy, J., and Coauthors, 2010: Towards prediction of decadal climate variability and change. *Procedia Environ. Sci.*, **1**, 287–304, doi:10.1016/j.proenv.2010.09.018.
- Neitsch, S. L., J. G. Arnold, J. R. Kiniry, and J. R. Williams, 2005: Soil and Water Assessment Tool theoretical documentation, version 2005. Texas A&M University, 494 pp. [Available online at <http://swat.tamu.edu/media/1292/SWAT2005theory.pdf>.]
- Nigam, S., M. Barlow, and E. H. Berbery, 1999: Analysis links Pacific decadal variability to drought and streamflow in United States. *Eos, Trans. Amer. Geophys. Union*, **80**, 621–625, doi:10.1029/99EO00412.
- NRCS, 1994: State Soil Geographic (STATSGO) database: Data use and information. Miscellaneous Publ. 1492, USDA, 113 pp.
- Powell, J. W., 1879: *Report on the Lands of the Arid Region of the United States*. Government Printing Office, 195 pp. [Available online at <http://pubs.usgs.gov/unnumbered/70039240/report.pdf>.]
- Power, S., T. Casey, C. Folland, A. Colman, and V. M. Mehta, 1999: Interdecadal modulation of the impact of ENSO on Australia. *Climate Dyn.*, **15**, 319–324, doi:10.1007/s003820050284.
- Press, W. H., S. A. Teukolsky, W. T. Vetterling, and B. P. Flannery, 2007: *Numerical Recipes: The Art of Scientific Computing*. 3rd ed. Cambridge University Press, 1256 pp.
- Rayner, N. A., D. E. Parker, E. B. Horton, C. K. Folland, L. V. Alexander, D. P. Rowell, E. C. Kent, and A. Kaplan, 2003: Global analyses of sea surface temperature, sea ice, and night marine air temperature since the late nineteenth century. *J. Geophys. Res.*, **108**, 4407, doi:10.1029/2002JD002670.
- Rosenberg, N. J., 1987: Climate of the Great Plains region of the United States. *Great Plains Quart.*, **7**, 22–32.
- , 2007: *A Biomass Future for the North American Great Plains: Toward Sustainable Land Use and Mitigation of Greenhouse Warming*. Advances in Global Change Research, Vol. 27, Springer, 200 pp.
- , R. A. Brown, R. C. Izaurralde, and A. M. Thomson, 2003: Integrated assessment of Hadley Centre (HadCM2) climate change projections on agricultural productivity and irrigation water supply in the conterminous United States. *Agric. For. Meteorol.*, **117**, 73–96, doi:10.1016/S0168-1923(03)00025-X.
- Rosenthal, W. D., R. Srinivasan, and J. G. Arnold, 1995: Alternative river management using a linked GIS–hydrology model. *Trans. ASABE*, **38**, 783–790, doi:10.13031/2013.27892.
- Santhi, C., J. G. Arnold, J. R. Williams, W. A. Dugas, R. Srinivasan, and L. M. Hauck, 2001: Validation of the SWAT model on a large river basin with point and non point sources. *J. Amer. Water Resour. Assoc.*, **37**, 1169–1188, doi:10.1111/j.1752-1688.2001.tb03630.x.
- , N. Kannan, J. G. Arnold, and M. Di Luzio, 2008: Spatial calibration and temporal validation of flow for regional scale hydrologic modeling. *J. Amer. Water Resour. Assoc.*, **44**, 829–846, doi:10.1111/j.1752-1688.2008.00207.x.
- Schubert, S., and Coauthors, 2009: A U.S. CLIVAR project to assess and compare the responses of global climate models to drought-related SST forcing patterns: Overview and results. *J. Climate*, **22**, 5251–5272, doi:10.1175/2009JCLI3060.1.
- Smith, T. M., and R. W. Reynolds, 2004: Improved extended reconstruction of SST (1854–1997). *J. Climate*, **17**, 2466–2477, doi:10.1175/1520-0442(2004)017<2466:IEROS>2.0.CO;2.
- Spiegel, M. R., and L. J. Stephens, 2007: *Schaum's Outline of Statistics*. 4th ed. McGraw-Hill, 577 pp.
- Spruill, C. A., S. R. Workman, and J. L. Taraba, 2000: Simulation of daily and monthly stream discharge from small watersheds using the SWAT model. *Trans. ASABE*, **43**, 1431–1439, doi:10.13031/2013.3041.
- Srinivasan, R., and J. G. Arnold, 1994: Integration of a basin-scale water quality model with GIS. *J. Amer. Water Resour. Assoc.*, **30**, 453–462, doi:10.1111/j.1752-1688.1994.tb03304.x.
- , —, R. S. Muttiah, C. Walker, and P. T. Dyke, 1993: Hydrologic Unit Model for the United States (HUMUS). *Advances in Hydro-Science and Engineering*, S. Y. Yang, Ed., University of Mississippi Center for Computational Hydro-science and Engineering, 451–456.
- Thomson, A. M., R. A. Brown, N. J. Rosenberg, R. C. Izaurralde, D. M. Legler, and R. Srinivasan, 2003: Simulated impacts of El Niño/Southern Oscillation on U.S. water resources. *J. Amer. Water Resour. Assoc.*, **39**, 137–148, doi:10.1111/j.1752-1688.2003.tb01567.x.
- Ting, M., and H. Wang, 1997: Summertime U.S. precipitation variability and its relation to Pacific sea surface temperature. *J. Climate*, **10**, 1853–1873, doi:10.1175/1520-0442(1997)010<1853:SUSPVA>2.0.CO;2.
- Wang, H., and V. M. Mehta, 2008: Decadal variability of the Indo-Pacific Warm Pool and its association with atmospheric and oceanic variability in the NCEP–NCAR and SODA reanalyses. *J. Climate*, **21**, 5545–5565, doi:10.1175/2008JCLI2049.1.
- Weber, A., N. Fohrer, and D. Möller, 2001: Long-term changes of land use in a mesoscale watershed due to socio-economic factors—Effects on landscape functions. *Ecol. Modell.*, **140**, 125–140, doi:10.1016/S0304-3800(01)00261-7.
- Wilhite, D., 2000: *Drought: A Global Assessment*. Routledge, 168 pp.
- Winchell, M. W., R. Srinivasan, M. Di Luzio, and J. G. Arnold, 2007: ArcSWAT interface for SWAT2005 user's guide. USDA Agricultural Research Service, 431 pp.
- Wishart, D. J., 2004: *Encyclopedia of the Great Plains*. University of Nebraska Press, 940 pp.